

Hierarchical Representation for Chromatic Processing across Macaque V1, V2, and V4

Highlights

- Color-response blobs comprise a uniform architecture across V1, V2, and V4
- Blobs evolve progressively in spatial scale and separation of hue representation
- Two-photon imaging shows greater hue-specific cell clustering in V2 than in V1
- Chromotopic organization achieves greater spectral uniformity from V1 to V2 to V4

Authors

Ye Liu, Ming Li, Xian Zhang, ...,
Niall Mcoughlin, Shiming Tang,
Wei Wang

Correspondence

tangshm@pku.edu.cn (S.T.),
w.wang@ion.ac.cn (W.W.)

In Brief

How does our visual brain generate perceptual color space? Liu et al. find that within a uniform blob-like architecture of hue responses, chromotopic maps develop progressively in scale and precision along the visual hierarchy of macaque V1, V2, and V4. Such hierarchical refinement improves spectral uniformity, better reflecting color perception.

Article

Hierarchical Representation for Chromatic Processing across Macaque V1, V2, and V4

Ye Liu,^{1,2,9} Ming Li,^{3,9} Xian Zhang,^{1,4} Yiliang Lu,¹ Hongliang Gong,^{1,2} Jiapeng Yin,¹ Zheyuan Chen,¹ Liling Qian,¹ Yupeng Yang,⁵ Ian Max Andolina,¹ Stewart Shipp,¹ Niall McLoughlin,⁶ Shiming Tang,^{7,8,10,*} and Wei Wang^{1,2,10,11,*}

¹Institute of Neuroscience, Key Laboratory of Primate Neurobiology, Chinese Academy of Sciences Center for Excellence in Brain Science and Intelligence Technology, State Key Laboratory of Neuroscience, Chinese Academy of Sciences, Shanghai Center for Brain Science and Brain-Inspired Intelligence Technology, Shanghai 200031, China

²University of Chinese Academy of Sciences, Beijing 100049, China

³State Key Laboratory of Cognitive Neuroscience and Learning, Beijing Normal University, Beijing 100875, China

⁴Cold Spring Harbor Laboratory, Cold Spring Harbor, NY 11724, USA

⁵Chinese Academy of Sciences Key Laboratory of Brain Function and Diseases, School of Life Sciences, University of Science and Technology of China, Hefei 230027, China

⁶Division of Pharmacy and Optometry, Faculty of Biology, Medicine, and Health Science, University of Manchester, Manchester M13 9PL, UK

⁷Peking University School of Life Sciences and Peking-Tsinghua Center for Life Sciences, Beijing 100871, China

⁸IDG/McGovern Institute for Brain Research at Peking University, Beijing 100871, China

⁹These authors contributed equally

¹⁰Senior author

¹¹Lead Contact

*Correspondence: tangshm@pku.edu.cn (S.T.), w.wang@ion.ac.cn (W.W.)

<https://doi.org/10.1016/j.neuron.2020.07.037>

SUMMARY

The perception of color is an internal label for the inferred spectral reflectance of visible surfaces. To study how spectral representation is transformed through modular subsystems of successive cortical areas, we undertook simultaneous optical imaging of intrinsic signals in macaque V1, V2, and V4, supplemented by higher-resolution electrophysiology and two-photon imaging in awake macaques. We find a progressive evolution in the scale and precision of chromotopic maps, expressed by a uniform blob-like architecture of hue responses within each area. Two-photon imaging reveals enhanced hue-specific cell clustering in V2 compared with V1. A phenomenon of endspectral (red and blue) responses that is clear in V1, recedes in V2, and is virtually absent in V4. The increase in mid- and extra-spectral hue representations through V2 and V4 reflects the nature of hierarchical processing as higher areas read out locations in chromatic space from progressive integration of signals relayed by V1.

INTRODUCTION

Understanding how the spectral reflectance of a surface ultimately results in the perception of a color has been the remit of both scientists and artists over the centuries (Conway, 2012; Conway et al., 2010; Mollon, 2003). Human and macaque perceptual color space is three dimensional, inherent in the trichromatic sampling of the spectrum by long-, medium-, and short-wavelength (L, M, and S) sensitive cones in the retina. The chromatic plane of color space (Figure 1A) derives from two forms of cone opponency: L versus M, and S versus L+M, that are transmitted from retinal ganglion cells through parvocellular and koniocellular neurons in the lateral geniculate nucleus (LGN) before entering the early visual cortex for further processing (Chatterjee and Callaway, 2002; Hendry and Reid, 2000; Lennie et al., 1990; Martin et al., 1997; Roy et al., 2009). Cells in early visual cortex can only be tuned to discrete loci in color space by integrating signals from the parvo and konio channels (Conway,

2001; Conway et al., 2002; Conway and Livingstone, 2006; Horwitz and Hass, 2012; Hubel and Livingstone, 1987; Johnson et al., 2001, 2004, 2008; Kiper et al., 1997; Solomon and Lennie, 2005). The cytochrome oxidase (CO) blobs of V1 are the first cortical site of parvo and konio convergence. Single-unit electrophysiological studies of CO blobs have reported cell classes sensitive to either red/green or blue/yellow color contrast, the latter in a minority (Livingstone and Hubel, 1984), with some suggestion that individual blobs are dominated by one or the other (Landisman and Ts'o, 2002a; Ts'o and Gilbert, 1988). The canonical color pathway (Figure 1B) then relays from the CO blobs of V1 through CO thin stripes of V2 to color-specialized domains of V4 and posterior inferotemporal cortex (PIT) referred to as “globs” (Chen et al., 2008; Conway et al., 2007, 2010; Conway and Tsao, 2006; Harada et al., 2009; Landisman and Ts'o, 2002b; Li et al., 2014; Livingstone and Hubel, 1984; Lu and Roe, 2008; Sincich and Horton, 2005a; Tanigawa et al., 2010; Xiao et al., 2003, 2007) and further anterior patches (Komatsu

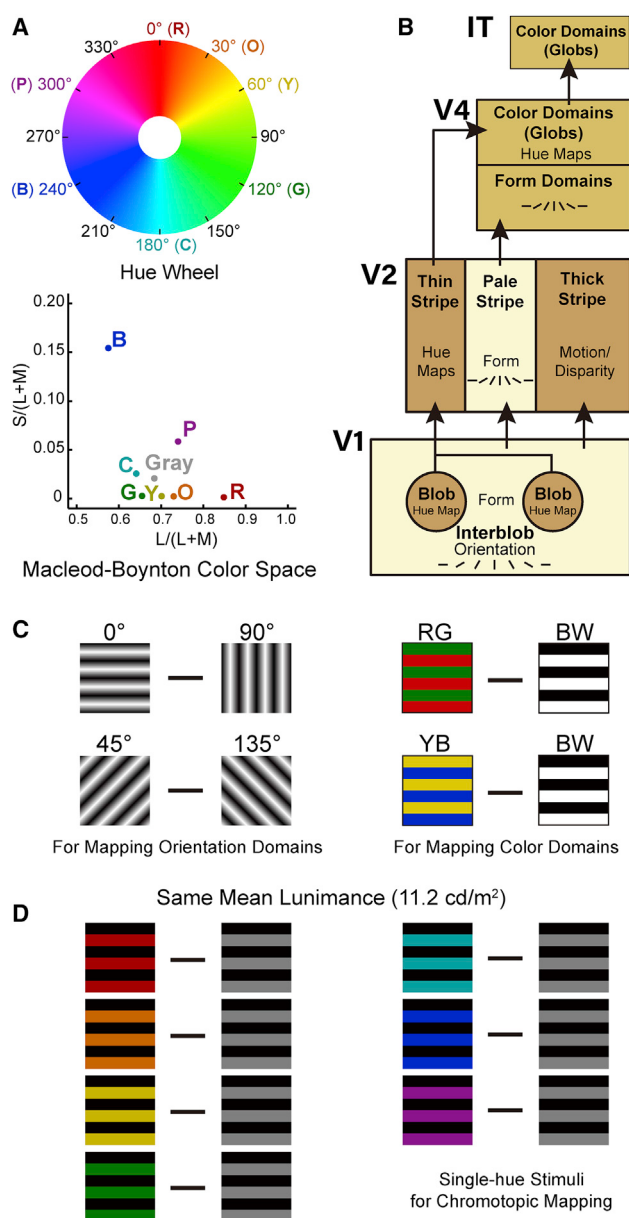


Figure 1. Schematics of Color Space, the Ventral Visual Stream, and Visual Stimulus Sets

(A) Hue wheel (top) is one dimension shared by both hue-saturation-lightness (HSL) and hue-saturation-value (HSV) color spaces. The hues of red (R), orange (O), yellow (Y), green (G), cyan (C), blue (B), and purple (P) in this study are defined in degrees as in the hue wheel. Tested hues are replotted in Macleod-Boynton color space (bottom) to illustrate their differential cone excitations.

(B) Anatomical modular substructure of parallel pathways within the V1-V2-V4-IT hierarchy; physiologically, color and orientation information are not mutually exclusively encoded.

(C) Achromatic and dual-hue stimuli used to map orientation and color domains.

(D) Stimuli of isoluminant square-wave color gratings used for chromatopic mapping.

See also Table S1 and Figure S1.

et al., 1992; Lafer-Sousa and Conway, 2013). How this integration of chromatic information is subserved by anatomical color pathways has yet to be fully resolved.

Hue is a quantitative perceptual attribute of color commonly used to describe the stimulus position within the visible spectrum (Figure 1A). As “color processing,” broadly defined, can incorporate a contribution to cue-invariant form vision, we refer more narrowly to spectral hue processing that, empirically, we attribute to modules better activated by chromatic contrast than achromatic luminance contrast. Previous optical imaging of intrinsic signal (OIS) studies adopting this criterion have confirmed the co-localization of chromatic response domains with CO blobs in V1 and thin CO stripes in V2 (Landisman and Ts'o, 2002b; Lu and Roe, 2008; Xiao et al., 2003) and the segregation of such modules in V4 (Tanigawa et al., 2010). Hue maps have been separately recorded in V1 blobs (Xiao et al., 2007), V2 thin stripes (Lim et al., 2009; Xiao et al., 2003), and V4 color domains (Conway and Tsao, 2009; Li et al., 2014; Tanigawa et al., 2010). These hue maps appear to be organized in a chromotopically structured manner; i.e., similar hues activate neighboring cortical positions, but how they reflect perceptual color space is unknown. In addition, the response of intrinsic signals are heavily biased in favor of red and blue hues, particularly in V1 (Valverde Salzmann et al., 2012; Xiao et al., 2007). This endspectral response within V1 and its CO blobs, first reported utilizing the 2DG technique even after equating relative saturation (Tootell et al., 1988), was also reported in human fMRI (Nasr and Tootell, 2018). A recent study using 2-photon calcium imaging confirms the preponderance of cells preferring red and blue hues in V1, while failing to identify chromatic heterogeneity among blobs (Garg et al., 2019).

We may conceive of an idealized cortical hue map as isometrically organized, whereby hue responses are equally weighted and the spatial organization of cortical hue-response loci approximates the planar metric of perceptual color space. What remains unclear is how hue maps within the anatomical color modules evolve with hierarchical processing from V1 to V4—given that single units sampled at a still higher level (PIT cortex) do appear to provide a more uniform representation of perceptual color space (Bohon et al., 2016). Does the chromatopic pattern of response in V1 persist or transform into something closer to the idealized isometric organization defined above? To address these questions, we probed spectrally specific responses with various chromatic stimuli (Figures 1A, 1C, and 1D), performing simultaneous intrinsic optical imaging of V1, V2, and V4 in the same anesthetized macaque preparation, allied to electrophysiological recordings (V1, V2, and V4) and 2-photon imaging (V1 and V2) in awake macaques. Deploying multiple techniques across these cortical areas enables us to quantify the similarities and differences at both cellular and population levels, examining how spectral responses develops progressively along the primate ventral visual pathway.

RESULTS

Mapping Color-Response Domains across V1, V2, and V4

We first used either red/green (RG) or blue/yellow (BY) gratings matched to achromatic gratings to reveal chromatic response

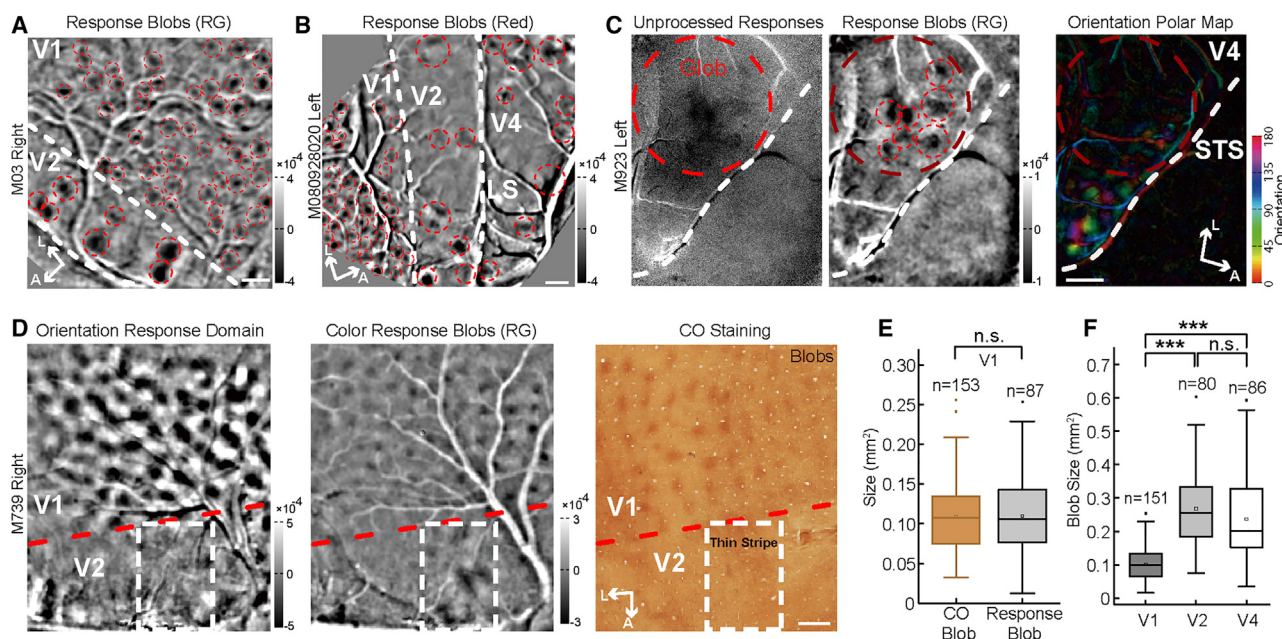


Figure 2. Color-Response Blobs in V1, V2, and V4

(A) Color-response blobs evoked by RG gratings, circled by red dotted lines, in V1 and V2.
 (B) Simultaneous recording of color-response blobs evoked by red stimulus in V1, V2, and V4.
 (C) Color-response blobs (middle, after standard spatial filtering) within a V4 glob (left). The outline of the glob transposed to an orientation polar map of the same V4 region (right) demonstrates non-overlapped response domains.
 (D) Differential orientation and color-response maps and histological CO staining of the corresponding region.
 (E) Boxplots of sizes of CO staining blobs and color-response blobs in V1 from 3 hemispheres (n.s., p > 0.05, Wilcoxon rank-sum test; n, blob numbers).
 (F) Comparison of response blob sizes in V1, V2, and V4 from 7 hemispheres (Wilcoxon rank-sum test with Bonferroni correction, ***p < 0.001).
 A, anterior; L, lateral; LS, lunate sulcus; STS, superior temporal sulcus. Scale bars, 1mm. See also Figures S1 and S2.

domains (Figures 2A–2C and S1). Figure S1A shows an example where RG stimulation strongly activated blob shaped color-response domains in V1, V2 thin stripes, and V4, avoiding direct, concentric overlap with orientation-response domains, as previously reported (An et al., 2012; Lu and Roe, 2008; Tanigawa et al., 2010). Similar segregated activations in V2 and V4 are shown for a second example with the orientation responses displayed as a polar orientation map (some fainter orientation responses are visible within the color domains; Figure S1B). In summary, our results are consistent with earlier single-unit recordings and optical imaging data (Landisman and Ts'o, 2002b; Livingstone and Hubel, 1984; Lu and Roe, 2008; Tanigawa et al., 2010; Xiao et al., 1999), in demonstrating modular subsystems for processing color across macaque V1, V2, and V4.

A Uniform Blob-like Architecture of Color Responses across V1, V2, and V4

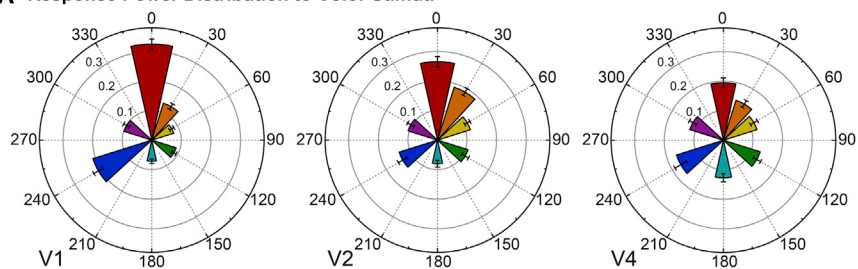
The color-response domains concurrently activated by RG gratings are blob-like, notably larger, and more widely spaced in V2 than in V1 (Figure 2A). Likewise, Figure 2B shows co-activated color-response blobs across V1, V2, and V4. The domain size of unprocessed V4 color responses (Figure 2C) was substantially larger, roughly equating in scale to the color “globs” measured at several millimeters in diameter by fMRI (Conway et al., 2007). The smaller foci that we refer to as color-response blobs emerged after further processing. This finding of the color-

response blobs within each area was common to all animals examined (Figures S2A and S2B).

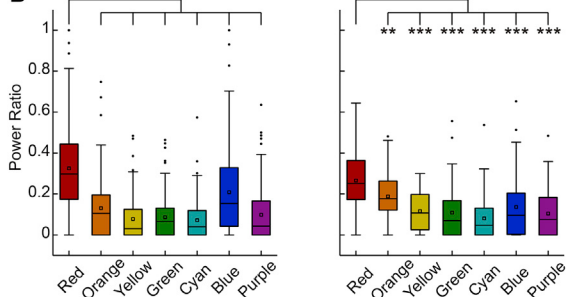
The sum activation achieved by our set of seven single-hue stimuli (red, orange, yellow, green, cyan, blue, and purple) should theoretically provide a better index of color-response domain size than the partial activation revealed by RG gratings alone. These single-hue stimuli were square-wave gratings coupled to an achromatic grating of matching luminance contrast and spatial frequency (SF; Figure 1D) aiming to elicit maximal neural responses from the surface of cortex containing single- and double-opponent color-sensitive cells (Friedman et al., 2003; Johnson et al., 2001, 2004, 2008; Kiper et al., 1997; Lennie et al., 1990). The sizes of color-response blobs were compiled from the envelope of the response domains elicited by single-hue stimuli, where all pixels exceeded a threshold response level at three standard deviations (SDs) above the baseline (see STAR Methods).

This criterion of physiological measurements was verified for V1 in conjunction with V1 histological CO-staining from three hemispheres (an example case is shown in Figure 2D). CO blob boundaries were determined by standard image-processing methods (An et al., 2012; Sincich and Horton, 2005b). The average diameter of blobs was $292 \pm 5 \mu\text{m}$ (mean \pm SE), consistent with previous reports (Farias et al., 1997; Solomon, 2002). The image alignment gave an average shift of $91 \pm 36 \mu\text{m}$ (mean \pm SD) between a CO blob and the corresponding color-response blob (attributable to differential histological

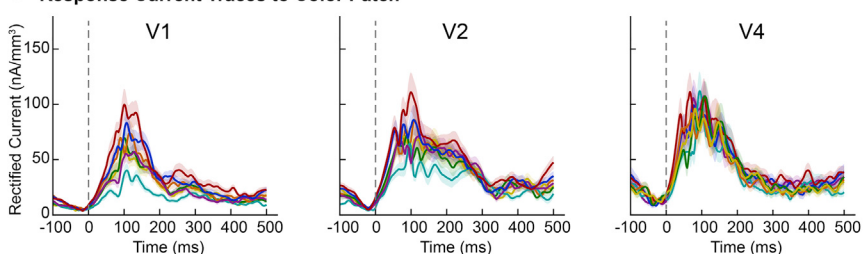
A Response Power Distribution to Color Stimuli



B



C Response Current Traces to Color Patch



D

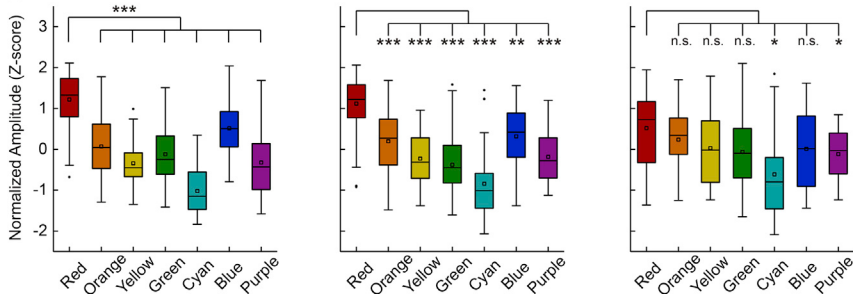


Figure 3. Comparison of Population Responses between Red and Other Hues in V1, V2, and V4

(A) Rose plots of response power ratio ($\text{mean} \pm \text{SE}$) of hues. The response power ratios varies among the seven hues within each area (V1 and V2, $p < 10^{-6}$; V4, $p = 0.0165$; bootstrap, details in **STAR Methods**), but the uniformity of the overall distribution of color responses increases monotonically from V1 to V2 and V4 ($p < 10^{-6}$ for all comparisons, bootstrap).

(B) Comparison of response power ratio between red and other hues (** $p < 0.001$, ** $p < 0.01$, * $p < 0.05$, n.s., $p > 0.05$, Wilcoxon rank-sum test with Bonferroni correction).

(C) The traces of average rectified currents to single-hue patch stimuli. Gray dashed line: stimulus onset; shaded regions: SE of current across channels. Data are from 51, 36, and 24 recording channels in supragranular layers from each area.

(D) Comparison of rectified current amplitudes between red and other hues (Wilcoxon signed-rank test with Bonferroni correction). The current amplitudes are Z score normalized within each recording channel.

See also [Figures S3](#) and [S4](#).

equivalent in V2 and V4 but significantly larger than those in V1 ([Figure S2C](#)). In summary, the functional architecture of color-response blobs in V1 is retained hierarchically across V2 and in V4, with a larger blob size in both areas.

The Evolution of Hue Representation from V1 to V4

A major aim of this study was to investigate how color signals are transformed across three successive visual areas. Previous studies have demonstrated endspectral response bias in V1 ([Garg et al., 2019](#); [Tootell et al., 1988](#); [Valverde Salzmann et al., 2012](#); [Xiao et al., 2007](#); [Yoshioka and Dow, 1996](#)), so we asked whether this response asymmetry ex-

shrinkage)—comparable to a previous study using the same method ([Valverde Salzmann et al., 2012](#)). After correcting for histological shrinkage of the imaged tissue, CO blobs were similar in size to color-response blobs set at the 3-SD criterion. [Figure 2E](#) shows that there was no statistical difference in their mean area size (CO blob: $0.109 \pm 0.003 \text{ mm}^2$, V1 response blob: $0.105 \pm 0.004 \text{ mm}^2$, mean \pm SE), empirically validating our procedure for measurement of color-response blob size in V1. Applying the same criterion, we found that the sizes of color blobs in V2 ($0.268 \pm 0.013 \text{ mm}^2$) and V4 ($0.235 \pm 0.014 \text{ mm}^2$) were comparable, and that both were significantly larger than those in V1 ([Figure 2F](#)). We note, in addition, that the cortical organization of orientation preference domains obeys a similar size principle. The sizes of concurrently recorded orientation domains are

tends to V2 and V4. To examine the same population of color-response blobs identified by the procedures described above (151 blobs in V1, 80 in V2, and 86 in V4), we defined the individual hue response power as the product of the strength and the size of response to each hue within each color-response blob (i.e., the mean pixel signal strength multiplied by the number of pixels activated by each hue). We then computed the power ratio of each hue as the response power for that hue divided by the sum of all the response powers within the same color-response blob. Finally, averaging across all color-response blobs within each area, we obtained mean response power ratios for V1, V2, and V4, shown as a rose plot in [Figure 3A](#). As expected, in V1 the priority of red, followed by blue is obvious. However, this endspectral response lessens in V2 and is further diminished

in V4 where the hue response profile is statistically more uniform than V1 and V2. Boxplots verify that the mean response power ratio is significantly greater to red than to other hues in both V1 and V2 and that this precedence wanes in V4 (Figure 3B). The priority of blue to the five hues other than red is notable in V1 but absent from V2 and V4 (Figure S3A).

Intrigued by this outcome, we added a complementary analysis of spectral variation of LFP responses recorded in a separate study of alert animals. Figures 3C and S3C show average rectified current traces obtained in LFP recordings from supragranular layers in V1, V2, and V4. Statistical comparison (Figure 3D) of current amplitude between red and other hues shows the current amplitude to red is largest in V1 and V2 but attains parity with most other hues in V4. Similar to intrinsic signals, in V1 we find that blue is inferior to red while ranking above the other hues but loses this status in V2 and V4 (Figures S3B and S3D). A sample of single unit data from the same awake monkey recordings (Figure S4) reflects the same pattern observed in population recordings from both intrinsic signals and LFP responses, demonstrating that the population hue response changes from one of endspectral dominance in V1 to a markedly more uniform distribution in V4.

How Do Hue Signals Map onto Individual Cells in V1 and V2?

To establish population responses at single-cell resolution, we applied 2-photon calcium imaging in V1 and V2 of two alert monkeys. Experiments were conducted using the identical set of seven test hues, here taking the form of small, static patches iso-luminant to the achromatic background. In 2-photon imaging, we recorded 3,608 visual-responsive V1 neurons (one-way ANOVA, $p < 0.05$) and 233 visual-responsive V2 neurons from one monkey, and 6,202 visual-responsive V2 neurons from a second monkey. Figure 4A illustrates the calcium responses of six cells sampled from a color blob in either area, showing various forms of spectral tuning. The population of cells recorded at each site, coded by preferred hue, is shown in Figure 4B. Cell counts of preferred hues across all sampled sites in either area show that the frequency of cells preferring red and blue is larger than for all other hues (Figure S5A). For V1, these results are consistent with our findings above and previous population (Tootell et al., 1988; Valverde Salzmann et al., 2012; Xiao et al., 2007) and single-cell studies (Garg et al., 2019). For V2, the excess of blue cells in V2 is less prominent than in V1 (χ^2 test, $p < 0.001$) while the representation of midspectral hues is correspondingly enhanced.

While the endspectral bias is modestly diminished in the V2 sample with respect to V1, the topography of hue clustering is much enhanced (Figure 4B). In V1 loose red and blue clusters are visible, while the remaining hues are distributed more sporadically. By contrast, in V2, the subsets of cells preferring the minority hues (particularly orange, green, and purple) occupy clearly defined sub-zones, with some interspersion at their boundaries. One numerical indication of enhanced clustering in V2 compared to V1 is given by the increase in peak density for cells preferring minority hues, particularly green, as shown in Figures 4C and 4D. For more rigorous quantification of this change in chromatic organization from V1 to V2, we

adopted a “cluster index,” initially introduced to examine the organization of orientation and SF maps obtained by 2-photon imaging of macaque V1 (Nauhaus et al., 2012). The cluster index measures the spatial scale of congregation of similarly tuned cells by charting the fall-off in correlation of tuning properties between cell pairs located increasingly far apart. The index is normalized by the average correlation of randomly selected cell pairs within the inspected field (as delimited in Figure 4B). A cluster index equal to 1 suggests that neurons with different preferences are randomly scattered in a salt-and-pepper manner. Thus, the decline of the index toward a value of 1.0 quantifies how hue preferences change from more similar to less similar across the cortical surface. The orientation preference map of V1 is regarded as being a highly ordered map showing smooth transitions of orientation preferences across the brain surface. So as a comparison, we first computed the cluster index for V1 orientation responses in the same recording chamber as the color responses (Figure 4E). The orientation cluster index (Figure 4F) is consistent with the previous report (Nauhaus et al., 2012), demonstrating systematic change of orientation preferences along the cortical surface. In contrast to orientation responses, the V1 color responses have much lower indices. However, the cluster index for V2 chromotopic map is in a similar range as that for V1 orientation preference map, demonstrating greater hue-specific cell clustering in V2 than in V1. To better visualize this change of hue preferences, we generated a larger field of view constructed from four adjacent sampling windows in V2 (Figure 4G).

Characteristics of Hue Maps within V1, V2, and V4

Endspectral responses evidently distorts the metrics of hue-mapping, and the lessening of this bias through V2 and V4 could be taken to signify an orderly synthesis of perceptual color space. To quantify the changes in precision of chromotopic organization more rigorously we examined color-response domains in V1, V2, and V4 co-activated by single hue stimuli, seeking to measure the relationship between hue cortical positions and corresponding hues in perceptual color space (Figure 1A).

Chromotopic Precision and Scale Increase from V1 to V2 and V4

Using identical procedures to previous studies (Li et al., 2014; Xiao et al., 2003, 2007), the locus of peak response for each hue was defined as the contour at 75% of peak signal strength (Figure 5A), to generate hue maps by their superimposition (Figure 5B). By summing the number of hue regions per domain, the mean values were very close: V1: 4.93 ± 0.13 ($n = 151$); V2: 5.45 ± 0.16 ($n = 80$); V4: 5.15 ± 0.18 ($n = 86$). Note that some hue maps encode all seven hues tested while others are empirically incomplete (e.g., due to occlusion by blood vessels), as also observed in previous studies of V1, V2, and V4 (Li et al., 2014; Tanigawa et al., 2010; Xiao et al., 2003, 2007). We further noticed that many hue maps across all three areas are rainbow like in their sequence of hue responses. To better relate our results to previous studies, we first sought to quantify this chromotopic organization with respect to a linear hue metric, performing a regression analysis of cortical distance against hue distance for all possible pairs of co-activated hues (omitting maps with

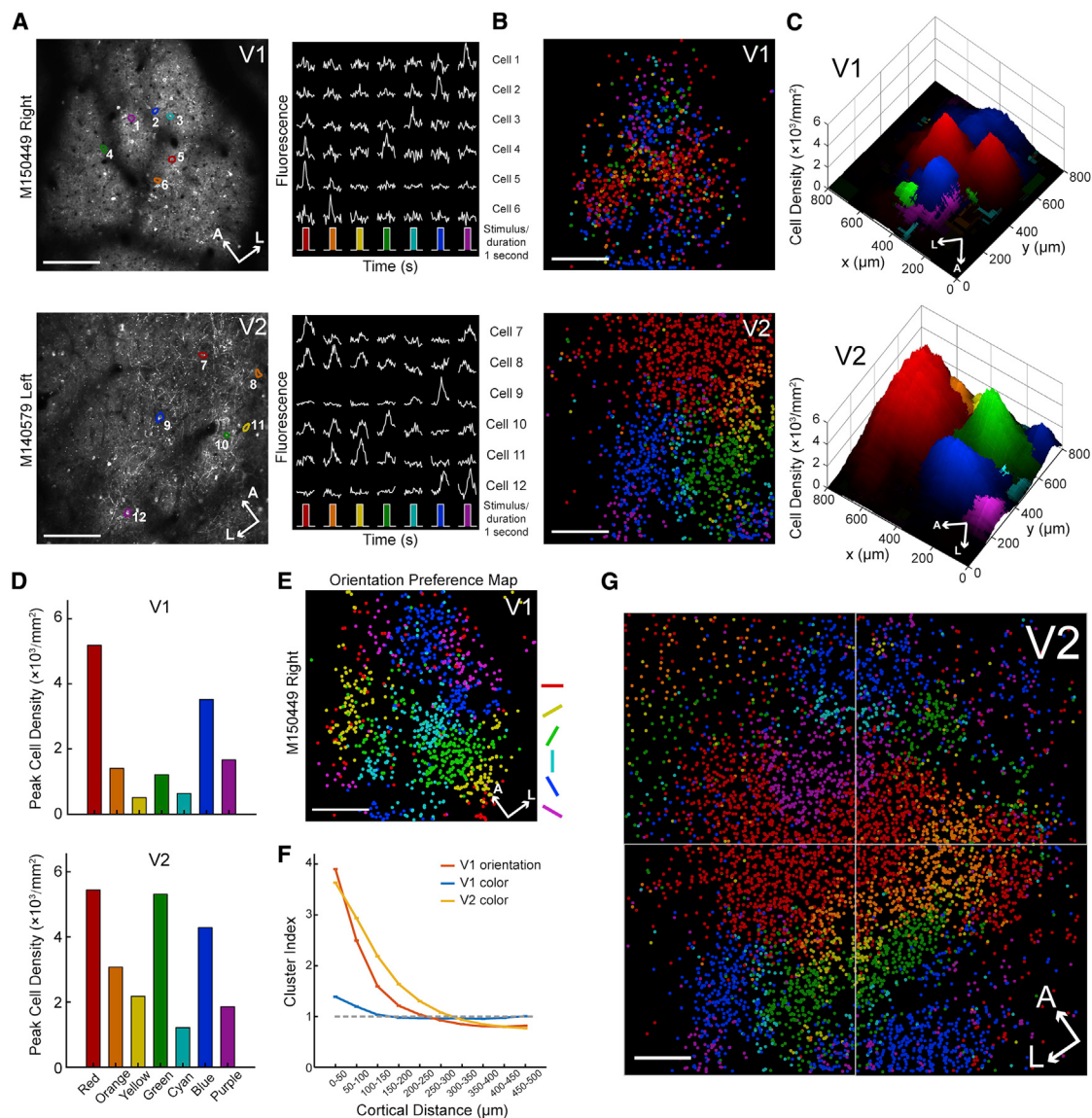


Figure 4. Hue Preferences of V1 and V2 Cell Clusters in 2-Photon Calcium Imaging

- (A) Fluorescence of a sample window (left) with blank stimulus, and fluorescence traces (right) of 6 sample cells in each area.
 - (B) Cell-distribution maps in V1 and V2 from the same frames in (A) illustrating cell clustering according to their preferred hues. Cells recorded across cortical depths of 100~500 μm (V1) or 100~325 μm (V2).
 - (C) 3D Plots of Color Cell Density Maps in V1 and V2 shown in (B). The 2D cell distribution maps are filtered by a square window of $0.125 \times 0.125 \text{ mm}^2$ (step size: 1 pixel, 1.5625 μm). The z axis represents the density ($\times 10^3/\text{mm}^2$) of cells preferring each hue in the x-y coordinates.
 - (D) Peak density of cells in each of the hue-specific cell clusters shown in (B).
 - (E) 2-photon orientation preference map in V1. 1,012 orientation-selective cells were collected across cortical depths of 100~500 μm .
 - (F) Cluster index comparison for hue and orientation preference cells in (B) and (E). Clustering indices significantly larger than 1 within distance of 250, 150, and 300 μm for V1 orientation, V1 color, and V2 color cells, respectively ($p < 0.001$, bootstrap with 1,000 trials of resampling).
 - (G) Hue-preference map over a larger scale of V2. The hue-preference map in the bottom left white box is illustrated in (B).
- A, anterior; L, lateral. Scale bars: 200 μm . See also Figure S5.

fewer than four different hue loci). The hue metric was generated from the hue circle (Figure 1A) linearized by a discontinuity at whichever location yielded the maximal regression coefficient (see Figures S5B–S5D for methodology and examples). Across areas we found that a rising fraction of hue maps—42%

(51/122), 54% (39/72), and 58% (38/65) in V1, V2, and V4, respectively—passed threshold criteria for regression analysis, randomization, and permutation tests ($p < 0.05$, which also applies to planar color metrics), but these proportions did not demonstrate a significant difference (Figure S5E).

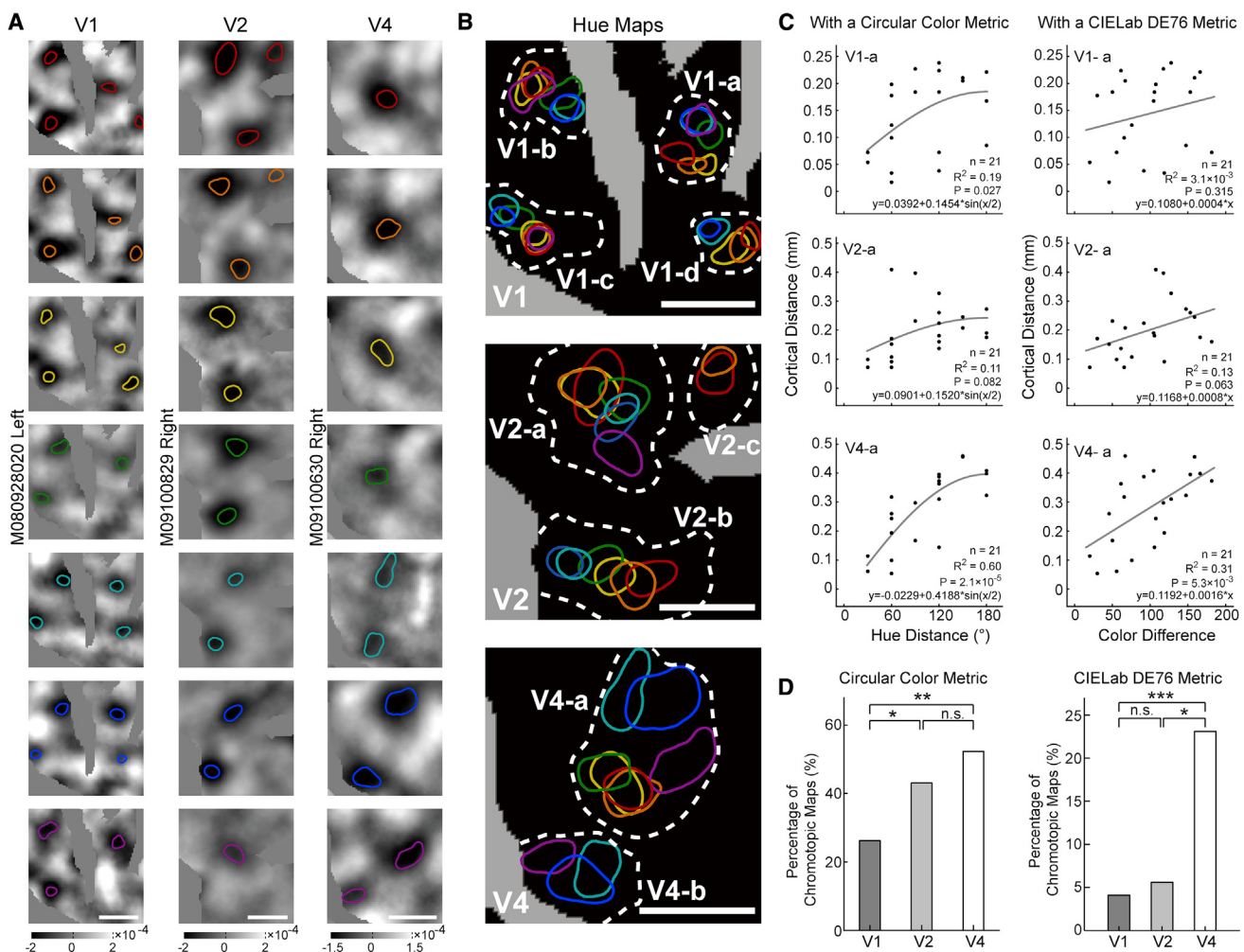


Figure 5. Orientation Selectivity Index Hue Maps in V1, V2, and V4

(A) Loci of peak activity areas evoked by single-hue stimuli.

(B) Hue maps combining the peak activity loci of V1, V2, and V4, respectively, illustrated in (A). The white dotted contours envelope all color responses at the criterion of 3SD above baseline.

(C) Regression analysis of cortical hue distances in color blobs against hue distances in a circular color metric (left) and CIELab DE76 metric (right) for V1-a, V2-a, and V4-a in (B). The curvature of regression with circular color metric reflects the sinusoidal function of geometric length against hue distance. n, R² and P: sample number, coefficient of determination and p value.

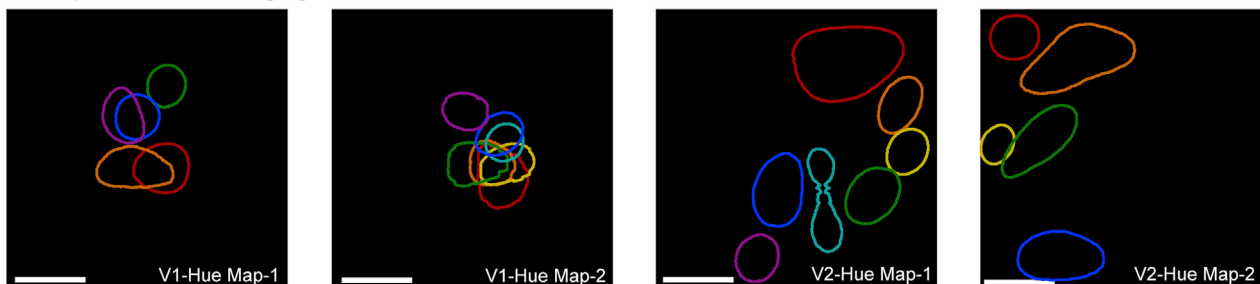
(D) Percentage of hue maps V1, V2, and V4 satisfying criteria in respect of the circular hue metric (left) and CIELab DE76 metric (right). ***p < 0.001; **p < 0.01; *p < 0.05; n.s., not significant; χ^2 test with Bonferroni correction.

Scale bars: 0.5 mm. See also Figure S5.

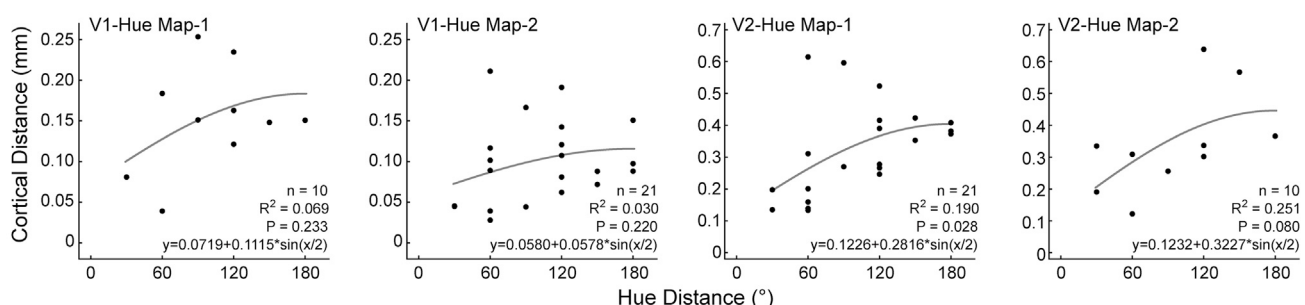
However, perceptual color space is known to be planar, and so we performed a similar regression analysis using a simple circular hue metric: specifically the geometric distance between a pair of hue loci, as if the hue circle of Figure 1A were perfectly transcribed upon the cortical surface. As shown in Figure 5C (the left panel), this metric also met with mixed success in predicting the configuration of cortical hue maps. Overall, 25% (31/122), 43% (31/72), and 52% (34/65) of intrinsic-signal hue maps in V1, V2, and V4, respectively, passed the threshold for significance. The proportion of significant hue maps in V2 and V4 statistically exceeds that in V1 (Figure 5D, the left panel). Whereas only a small fraction of maps (such as V4-a in Figure 5)

are fully circular upon casual inspection, this analysis demonstrates a hierarchical increase in “circularity” as a component of chromotopic organization. Finally, for a third measure, we resorted to CIELab (Table S1), a planar color space in which hue separation is more regularized in respect of hue discriminability. Using hue distances specified by the DE76 metric of CIELab space (Figure 5C, the right panel), we found that 4.1% (5/122), 5.6% (4/72), and 23.1% (15/65) of hue maps in V1, V2, and V4, respectively, passed the threshold level. While, under this criterion, the overall frequency of significant hue maps has diminished, the proportion in V4 remains significantly higher than that in the antecedent areas (Figure 5D, the right panel). In

A Hue Maps in 2-Photon Imaging



B With a Circular Color Metric



With a CIELab DE76 Metric

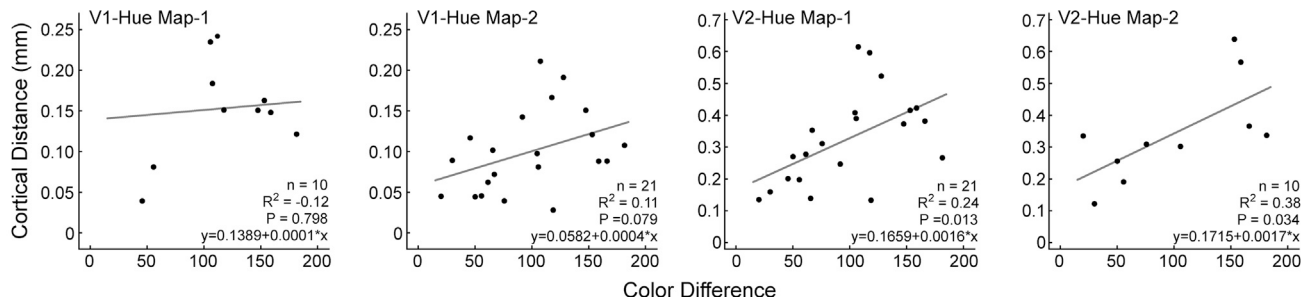


Figure 6. 2-Photon Calcium Imaging Hue Maps in V1 and V2

(A) Loci of 75% peak cell density areas in V1 and V2 evoked by single-hue patch stimuli. Scale bars: 200 μ m.

(B) Scatterplots illustrate the regression analysis for the maps in (A) using a circular color metric (top) and CIELab DE76 metric (bottom).

See also Figure S5.

summary, it seems fair to conclude that, while, up to the level we studied, a typical cortical hue map may lack a high-fidelity relationship to the organization of perceptual color space, there is nonetheless a demonstrable enhancement in the chromotopic precision from V1 to V2 to V4 that is recognizably “perceptual” in character.

We derived equivalent hue maps in V1 and V2 from 2-photon imaging; Figure 6A illustrates two examples from each area. Applying the identical set of regression analyses, we found that all four hue maps from these areas passed the statistical threshold in respect of the linearized color metric, but only the hue maps in V2 did so for the two planar color metrics (Figures 6B and S5F). We therefore note good consistency between the intrinsic-signal and 2-photon data, although the limited sample size of the 2-photon dataset precluded statistical comparison of the frequency of significant hue maps in V1 and V2 as visualized by this form of imaging.

Finally, we used the regression slope of hue maps as an index of the scale of chromotopic organization. For the hue-circle metric, we found that hue response loci were spaced further apart in V2 and V4, as reflected by significantly larger regression slopes: V1, $241 \pm 11 \mu\text{m}$; V2, $364 \pm 23 \mu\text{m}$; V4, $362 \pm 28 \mu\text{m}$; Wilcoxon rank-sum test with Bonferroni correction, V1 versus V2 $p < 1.4 \times 10^{-5}$; V1 versus V4: $p < 1.3 \times 10^{-3}$; V2 versus V4: $p = 0.79$. The larger scale of the hue maps is consistent with the larger color-response blob size we measured in V2 and V4. Taken together, these data demonstrate a hierarchical development in both the precision and scale of chromotopic mapping from V1 to V4.

Chromotopic Isometry Improves across V1, V2, and V4

We next outlined a parallel reduction in the anisometric spatial configuration of hue maps from V1 onward, based on the intrinsic-signal data. An analysis of the area of overlap between all pairs of hue responses in the color blobs (expressed as

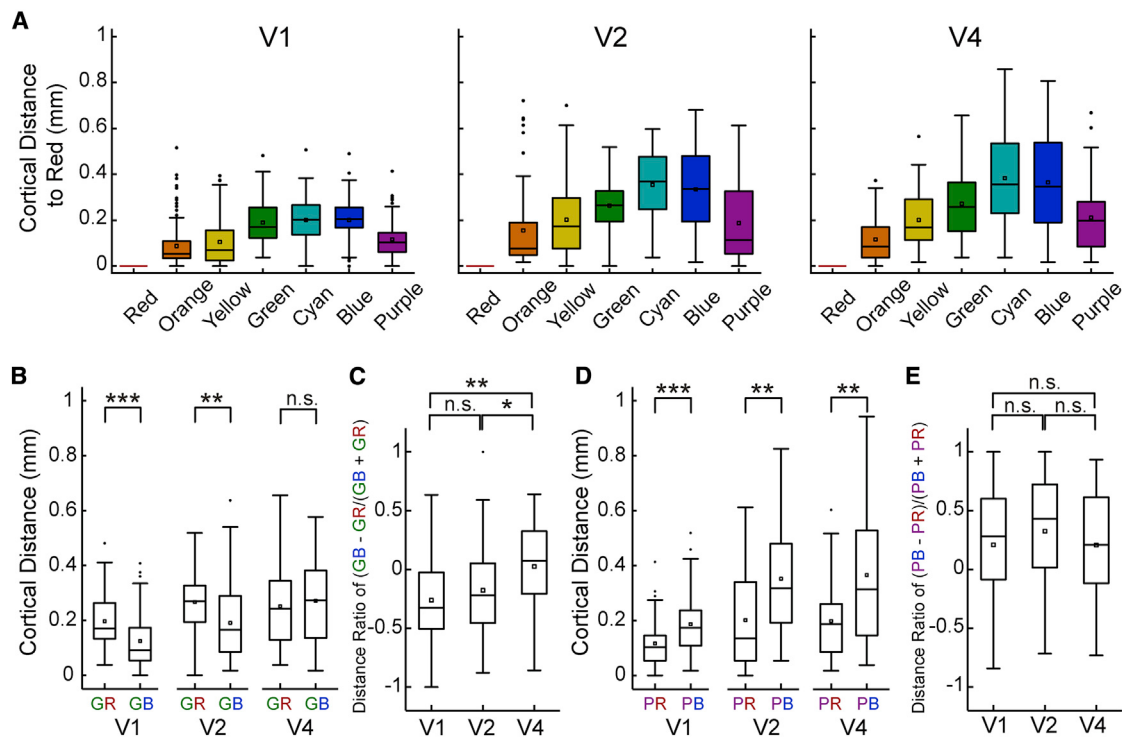


Figure 7. The Peak-to-Peak Distance between Hue Response Contours within Color Blobs in V1, V2, and V4

(A) The distances between red and other hues. Data are from 125, 69, and 63 chromotopic maps containing responses of red and at least one other color in V1, V2, and V4, respectively.

(B) Comparison of green-red (GR) and green-blue (GB) distances (**p < 0.001, **p < 0.01, n.s.: p > 0.05, Wilcoxon signed-rank test).

(C) Comparison of distance difference ratios as (GB-GR)/(GB+GR) (*p < 0.05, Wilcoxon rank-sum test with Bonferroni correction). Data in (B) and (C) are from 87, 46, and 41 chromotopic maps containing red, blue, and green responses in V1, V2, and V4, respectively.

(D) Comparison between purple-red (PR) and purple-blue (PB) distances (Wilcoxon signed-rank test).

(E) Comparison of distance ratios as (PB-PR)/(PB+PR).

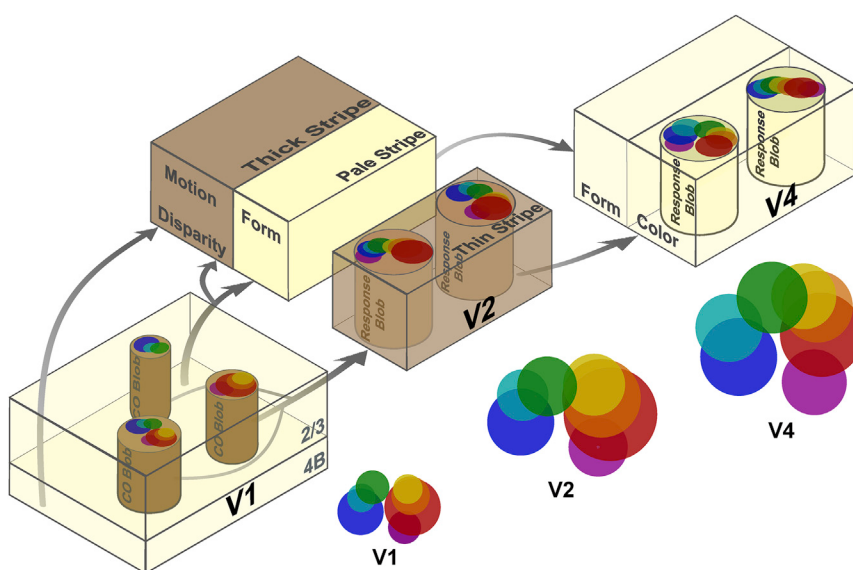
Data in (D) and (E) are from 67, 38, and 35 chromotopic maps containing red, blue, and purple responses in V1, V2, and V4, respectively.

See also Figure S6.

overlap ratios) proves most instructive (Figure S6A). It demonstrates that in area V1, red, orange, and yellow (ROY) hue responses have high mutual overlap, as do green, cyan, and blue (GCB), the two groupings being largely separate from one another. The seventh hue, purple, generally overlaps ROY (Figure S6A) but, alternatively, can associate with GCB (as seen, respectively, in hue maps V1-b and V1-c versus V1-a of Figure 5B). Figure S6B shows how these overlap ratios change from V1 to V2 and to V4. First, purple dissociates from the ROY group, particularly in V4. Second, the ROY and GCB groupings themselves partially desegregate, more markedly in the case of GCB. Green, in dissociating from cyan and blue, actually increases its overlap with ROY.

How do these changes in overlapping hue-response territories affect the spatial uniformity—i.e., the isometry—of the chromotopic gradient? We computed the peak-to-peak distances of hue contours within hue maps to define the separation of hues. The outcome (Figure 7A) shows that, while red and cyan or blue peak loci are maximally spaced apart in all three areas, the relative locations of the other hues undergo systematic shifts. Taking end spectral red and blue (rather

than the less frequent cyan) responses as robust markers for opposite poles of a hue map, we evaluated the relative distances of green and purple response loci from these poles. We found that the average cortical distance between green and blue (GB) is shorter than that between green and red (GR) in both V1 and V2 but not in V4 (Figure 7B). We normalized the difference between GB distance and GR distance as a ratio of (GB-GR)/(GB+GR), whereby a ratio near to zero indicates near equality between GB and GR. The ratio in V4 (median: 0.07) is closer to zero than that in V1 (median: -0.33) and V2 (median: -0.22) (Figure 7C). In other words, in V4 the green locus adopts an equi-distant position in cortical space, much as it does in planar hue space. The outcome of analogous tests with purple was different: although gaining a more autonomous response territory (Figure S6B), overall, purple maintains a relative proximity to red rather than blue (Figure 7D) within all three successive areas, with no significant change across V1, V2, and V4 (Figure 7E). Notably, however, the purple locus appears to “oscillate” between the red and blue poles, as reflected by the large variance in the boxplots of Figure 7D.



In summary, and particularly with reference to midspectral green hues, we infer that the spatial parameters of averaged chromatopic maps regularize in the transition from V1 to V2 to V4 (Figure 8), more closely approximating an isometric organization mirroring perceptual color space.

DISCUSSION

The functional operations associated with each hierarchical stage of color processing are not well established. Figure 8 illustrates a schematic integrating our findings with many previous studies, reflecting a classic “systems engineering” mindset for understanding brain function; namely, one in which parallel processing is implemented through discrete modules and serial processing operations traverse distinct hierarchical stages. Growing experience with deep neural networks suggests that the character of neural processing is not so uniformly lawful (Flachot and Gegenfurtner, 2018). While interpreting the hierarchical development of hue mapping as a progressive construction of perceptual color space, we accept that this proposal describes the main current, if not the eddies, in a flow of processing toward downstream sites beyond V4.

Architecture of Chromatic Processing across V1, V2, and V4

Commonly known as blobs, thin stripes, and “globs” in V1, V2, and V4 (Figures 1B and 8) (Conway et al., 2010), this study further reveals all these color-responsive domains actually comprise a uniform modular (or blob-like) architecture for color processing along the visual hierarchy, differing across areas chiefly in scale. Although the sizes of color-response blobs in V2 and V4 are comparable, they are on average much larger than those in V1 (Figures 2, S1, and S2). Our V4 globs match in size anatomically defined foci in a similar caudal sector of V4 receiving inputs from V2 thin stripes (Felleman et al., 1997; Xiao et al., 1999), and they are also commensurate with color-response regions identified in V4 and PIT by fMRI

Figure 8. Schematic of the Averaged Chromatopic Maps in V1, V2, and V4

The color-response blob is a conserved functional unit enlarging in scale from V1, V2 to V4. The figurative hue maps depict hierarchical evolution from V1 toward a more isometric hue map in V2 and V4. The size of each colored disk quantifies the response power ratio of each corresponding hue. The configuration of hue maps is the averaged peak-to-peak distance between hue responses within each area. The hue maps in blobs appear intuitively similar to pointillist paintings in which small, distinct dots of color are applied in patterns to form a cohesive image.

studies in macaques (Conway et al., 2007; Conway and Tsao, 2006; Harada et al., 2009; Lafer-Sousa and Conway, 2013; Rosenthal et al., 2018; Wade et al., 2008). The “size principle” of cortical functional organization applies

equally to orientation (Figures S1 and S2C), suggesting functional organization and connections in extra-striate visual cortices may be significantly different from V1. We note that the size of some larger color-response blobs in V1 encoding six or seven hues was about twice the average CO blob size, in potential correspondence to so-called “blob bridges” (Landisman and Ts’o, 2002a; Ts’o and Gilbert, 1988).

The definition of a “color response” is necessarily empirical, as the functional division of labor between parallel streams remains incompletely understood. For the 2-photon experiments, we defined it as selective response to hue; a substantial proportion of V1 cells combine this property with orientation selectivity (see Figure S7), consistent with a previous study (Garg et al., 2019). In the intrinsic-signal experiments a color response is the differential activation achieved by adding chromatic contrast to an achromatic square-wave grating matched in luminance contrast and SF; this activity should also include a component generated by oriented, hue-selective cells. Oriented and non-oriented hue-selective cells likely correspond to the double- and single-opponent classes described by single-unit studies (Johnson et al., 2001, 2004, 2008). Single-opponent cells should be activated by the chromatic phase of our square-wave gratings and double-opponent cells by the border contrast (Friedman et al., 2003), the latter response can exceed the former, at least as demonstrated by voltage-sensitive dye imaging in V1 (Zweig et al., 2015). Hence, at least in V1, we can attribute color responses (both 2 photon and intrinsic signal) to combined activity of double- and single-opponent cells; higher areas so far lack a similar level of consensus regarding color cell classification.

Inferences from the Evolution of Hue Maps across V1, V2, and V4: Cortical Construction of Color Space

The chromatic plane of color space is defined by polar coordinates of hue and saturation (with the orthogonal axis corresponding to lightness, or “value”). Or, more physiologically, by cartesian (“cardinal”) axes of chromaticity linked to the peripheral konio- and parvocellular systems, whose conjoint activity

must later be read out by cortical cells signaling discrete chromatic loci. Does this readout commence in the CO blobs of V1 where parvo and konio inputs first converge?

We found a surfeit of red and blue hue responses. This was seen in both our intrinsic-signal and 2-photon imaging data, the former echoing previous studies in macaque (Xiao et al., 2007, 2011), and marmoset (Valverde Salzmann et al., 2012), and the latter the recent report from Garg et al. (2019), also in macaques. Endspectral response bias in CO blobs was first detected by 2DG uptake experiments (Tootell et al., 1988) and later by electrophysiological recordings (Yoshioka and Dow, 1996). Significantly, all these studies employed computer monitors for color stimulation. Given the spectral emission characteristics of R, G, and B phosphors, endspectral bias looks to be the consequence of the fact that R and B phosphors elicit maximal cone-opponent responses (Mollon, 2009; Tootell et al., 1988): R in respect of L-M (parvo), and B in respect of M-L (parvo) and S-(L+M) (konio) (Figure 1A). This account of endspectral bias is corroborated by Valverde Salzman et al. (2012), who correlated the level of blob activation obtained by intrinsic-signal imaging with the L/M and S/(L+M) cone contrast produced by their test hues: they found that L/M contrast alone was a significant predictor of blob activity, and that it was their blue, rather than green stimulus that maximized M-L cone contrast.

The simplest model to account for the known segregation of red and blue responses—and moreover for the segregation of pooled purple, red, orange, and yellow responses from green, cyan, and blue, that we now report in V1 (Table S1; Figure S6)—is separate terminal foci for parvo afferents transmitting L-M and M-L signals. Exactly how konio signals contribute to this picture is uncertain. Valverde Salzman et al. were unable to observe blob activation driven by S cone contrast (i.e., konio signals) alone (Valverde Salzmann et al., 2012). We might infer that konio input contributes to our minority foci pooling purple with blue responses but have little hard evidence for integration of parvo and konio signals in V1; by contrast, the hue maps that we describe in V2 and V4 defy explanation without such integration.

Both forms of optical imaging confirmed that the pattern of endspectral dominance, characteristic of V1, receded in V2 and was virtually absent in V4 (Figure 3). The growth of mid-spectral and extraspectral hue representations in V2 and V4 implies functional convergence of parvo and konio signals, as arguable from closer consideration of the cellular hue map in V2 (Figure 4G). A cell receiving solely L-M parvo input that has a preferential response to an orange hue, rather than red, is conceivably “contrast tuned” for this input—analogous to a class of cell found in V4 that is similarly tuned for achromatic contrast (Sani et al., 2013). However, the purple and orange hues generate near identical levels of L-M cone contrast (see Figure 1A): contrast tuning for a sole L-M cone input should produce intermixed scattering of orange and purple hue preferring cells, on account of physiological noise, much as we observe in V1. The systematic, tight hue clustering seen in V2 precludes such an explanation based on sole channel contrast tuning; we infer, instead, that such narrow hue preferences depend upon dual input from the parvo and konio channels, and moreover sensitivity to a specific ratio of signal intensities, e.g., as modeled by multiplicative modulations

(Mehrani et al., 2020). It is both the spectral and the spatial properties of the cellular hue map that lead to this conclusion.

Complementary analysis showed that the hue maps in V2 and V4 are more isometric than in V1; they have greater uniformity in both the weighting and the spacing of separate hue responses. This is demonstrated by the centralizing shift of the green locus (Figure 7B). Even with random scatter, the “twin-spot” configuration of the hue responses in V1 (i.e., ROY versus GCB foci) would be sufficient to register a baseline incidence of significant hue mapping in respect of all three metrics that we tested. Notably, it was the two planar hue metrics (as opposed to the linearized one) that better demonstrated a rising prevalence of chromotopic organization through V2 to V4. In effect, hue maps develop from V1 to achieve a recognizably closer affinity to perceptual hue space in V4. This indicates that functional integration of the parvo and konio channels is a progressive process—one that might initiate to a minor extent in V1 and not yet be perfected at the level of V4. As presaged above, our systems engineer might stipulate (1) an initial stage registering activity in cardinal axes of chromatic space that is retinally specific (given that blobs are heavily monocular); (2) a second stage achieving a cyclopean representation of color contrast, and (3) a third stage at which surface hues (or spectral reflectances) are computed from the conjoint activity in the cardinal axes. Our observations suggest that color processing is not so rigidly implemented in a stage-wise, serial fashion. Nevertheless, the rationale for cortical maps of any description (e.g., visual, somatic, or acoustic) appeals to a minimization of wiring length to facilitate interactions between units tuned to nearby parameters of the mapped space (Barlow, 1986) and, on that basis, the evolution of cortical maps reflecting planar hue space acts as an index of perceptual color space undergoing hierarchical construction. This process is certain to extend beyond the zone of caudal V4 that we examined, since cells with narrow representations of hue and saturation continue to develop luminance-invariant and shape-invariant properties at stages located more anterior in area V4A, or IT cortex proper (Bohnen et al., 2016; Chang et al., 2017; Namima et al., 2014; Sanada et al., 2016).

STAR★METHODS

Detailed methods are provided in the online version of this paper and include the following:

- [KEY RESOURCES TABLE](#)
- [RESOURCE AVAILABILITY](#)
 - Lead Contact
 - Materials Availability
 - Data and Code Availability
- [EXPERIMENTAL MODEL AND SUBJECT DETAILS](#)
- [METHOD DETAILS](#)
 - Optical Imaging of Intrinsic-signal
 - Electrophysiological Recordings and Analysis
 - Histological Cytochrome-Oxidase Staining
 - Two-photon Imaging and Analysis
 - Analysis of Intrinsic Signals
- [QUANTIFICATION AND STATISTICAL ANALYSIS](#)

SUPPLEMENTAL INFORMATION

Supplemental Information can be found online at <https://doi.org/10.1016/j.neuron.2020.07.037>.

ACKNOWLEDGMENTS

This work was supported by the Strategic Priority Research Program of Chinese Academy of Sciences, Grant No. XDB 32060200 (to W.W.), the Shanghai Municipal Science and Technology Major Project, Grant No. 2018SHZDZX05 (to W.W.), National Natural Science Foundation of China Grant No. 31861143032 (to W.W.) and Grant No. 31730109 (to S.T.), and the Fundamental Research Funds for the Central Universities, Grant No. 2018NTST31 (to M.L.).

AUTHOR CONTRIBUTIONS

W.W. designed research; Y. Liu, M.L., X.Z., Y. Lu, H.G., J.Y., Z.C., L.Q., N.M., S.T., and W.W. performed research; N.M., Y.Y., S.S., and I.M.A. contributed analytic tools; Y. Liu, M.L., Y. Lu, J.Y., S.S., S.T., and W.W. analyzed data; Y. Liu, S.S., and W.W. wrote the main paper.

DECLARATION OF INTERESTS

The authors declare no competing interests.

Received: December 31, 2019

Revised: May 9, 2020

Accepted: July 28, 2020

Published: August 26, 2020

REFERENCES

- An, X., Gong, H., Qian, L., Wang, X., Pan, Y., Zhang, X., Yang, Y., and Wang, W. (2012). Distinct functional organizations for processing different motion signals in V1, V2, and V4 of macaque. *J. Neurosci.* 32, 13363–13379.
- Barlow, H.B. (1986). Why have multiple cortical areas? *Vision Res.* 26, 81–90.
- Bohon, K.S., Hermann, K.L., Hansen, T., and Conway, B.R. (2016). Representation of Perceptual Color Space in Macaque Posterior Inferior Temporal Cortex (the V4 Complex). *eneuro* 3, 0039-0016.2016.
- Bonhoeffer, T., and Grinvald, A. (1996). Optical imaging based on intrinsic signals: The methodology. In *Brain Mapping: The Methods*, A.W. Toga and J.C. Mazziotta, eds. (Academic Press), pp. 55–97.
- Chang, L., Bao, P., and Tsao, D.Y. (2017). The representation of colored objects in macaque color patches. *Nat. Commun.* 8, 2064.
- Chatterjee, S., and Callaway, E.M. (2002). S cone contributions to the magnocellular visual pathway in macaque monkey. *Neuron* 35, 1135–1146.
- Chen, C.M., Lakatos, P., Shah, A.S., Mehta, A.D., Givre, S.J., Javitt, D.C., and Schroeder, C.E. (2007). Functional anatomy and interaction of fast and slow visual pathways in macaque monkeys. *Cereb. Cortex* 17, 1561–1569.
- Chen, G., Lu, H.D., and Roe, A.W. (2008). A map for horizontal disparity in monkey V2. *Neuron* 58, 442–450.
- Chen, T.W., Wardill, T.J., Sun, Y., Pulver, S.R., Renninger, S.L., Baohan, A., Schreiter, E.R., Kerr, R.A., Orger, M.B., Jayaraman, V., et al. (2013). Ultrasensitive fluorescent proteins for imaging neuronal activity. *Nature* 499, 295–300.
- Chen, M., Yan, Y., Gong, X., Gilbert, C.D., Liang, H., and Li, W. (2014). Incremental integration of global contours through interplay between visual cortical areas. *Neuron* 82, 682–694.
- Conway, B.R. (2001). Spatial structure of cone inputs to color cells in alert macaque primary visual cortex (V1). *J. Neurosci.* 21, 2768–2783.
- Conway, B.R. (2012). Color consilience: color through the lens of art practice, history, philosophy, and neuroscience. *Ann. N Y Acad. Sci.* 1251, 77–94.
- Conway, B.R., and Livingstone, M.S. (2006). Spatial and temporal properties of cone signals in alert macaque primary visual cortex. *J. Neurosci.* 26, 10826–10846.
- Conway, B.R., and Tsao, D.Y. (2006). Color architecture in alert macaque cortex revealed by fMRI. *Cereb. Cortex* 16, 1604–1613.
- Conway, B.R., and Tsao, D.Y. (2009). Color-tuned neurons are spatially clustered according to color preference within alert macaque posterior inferior temporal cortex. *Proc. Natl. Acad. Sci. USA* 106, 18034–18039.
- Conway, B.R., Hubel, D.H., and Livingstone, M.S. (2002). Color contrast in macaque V1. *Cereb. Cortex* 12, 915–925.
- Conway, B.R., Moeller, S., and Tsao, D.Y. (2007). Specialized color modules in macaque extrastriate cortex. *Neuron* 56, 560–573.
- Conway, B.R., Chatterjee, S., Field, G.D., Horwitz, G.D., Johnson, E.N., Koida, K., and Mancuso, K. (2010). Advances in color science: from retina to behavior. *J. Neurosci.* 30, 14955–14963.
- Evans, R.M., Hanson, W.T., Brewer, W.L., and Twersky, V. (1954). Principles of Color Photography. *Phys. Today* 7, 18.
- Farias, M.F., Gattass, R., Piñón, M.C., and Ungerleider, L.G. (1997). Tangential distribution of cytochrome oxidase-rich blobs in the primary visual cortex of macaque monkeys. *J. Comp. Neurol.* 386, 217–228.
- Felleman, D.J., Xiao, Y., and McClendon, E. (1997). Modular organization of occipito-temporal pathways: cortical connections between visual area 4 and visual area 2 and posterior inferotemporal ventral area in macaque monkeys. *J. Neurosci.* 17, 3185–3200.
- Flachot, A., and Gegenfurtner, K.R. (2018). Processing of chromatic information in a deep convolutional neural network. *J. Opt. Soc. Am. A Opt. Image Sci. Vis.* 35, B334–B346.
- Friedman, H.S., Zhou, H., and von der Heydt, R. (2003). The coding of uniform colour figures in monkey visual cortex. *J. Physiol.* 548, 593–613.
- Gallant, J.L., Connor, C.E., Rakshit, S., Lewis, J.W., and Van Essen, D.C. (1996). Neural responses to polar, hyperbolic, and Cartesian gratings in area V4 of the macaque monkey. *J. Neurophysiol.* 76, 2718–2739.
- Garg, A.K., Li, P., Rashid, M.S., and Callaway, E.M. (2019). Color and orientation are jointly coded and spatially organized in primate primary visual cortex. *Science* 364, 1275–1279.
- Hansen, B.J., Eagleman, S., and Dragoi, V. (2011). Examining local network processing using multi-contact laminar electrode recording. *J. Vis. Exp.* 55, 2806.
- Harada, T., Goda, N., Ogawa, T., Ito, M., Toyoda, H., Sadato, N., and Komatsu, H. (2009). Distribution of colour-selective activity in the monkey inferior temporal cortex revealed by functional magnetic resonance imaging. *Eur. J. Neurosci.* 30, 1960–1970.
- Hendry, S.H.C., and Reid, R.C. (2000). The koniocellular pathway in primate vision. *Annu. Rev. Neurosci.* 23, 127–153.
- Horwitz, G.D., and Hass, C.A. (2012). Nonlinear analysis of macaque V1 color tuning reveals cardinal directions for cortical color processing. *Nat. Neurosci.* 15, 913–919.
- Hubel, D.H., and Livingstone, M.S. (1987). Segregation of form, color, and stereopsis in primate area 18. *J. Neurosci.* 7, 3378–3415.
- Hunt, R.W.G., and Pointer, M.R. (2011). Relations between Colour Stimuli. In *Measuring Colour*, M.A. Kriss, ed. (Wiley-Blackwell), pp. 41–72.
- Johnson, E.N., Hawken, M.J., and Shapley, R. (2001). The spatial transformation of color in the primary visual cortex of the macaque monkey. *Nat. Neurosci.* 4, 409–416.
- Johnson, E.N., Hawken, M.J., and Shapley, R. (2004). Cone inputs in macaque primary visual cortex. *J. Neurophysiol.* 91, 2501–2514.
- Johnson, E.N., Hawken, M.J., and Shapley, R. (2008). The orientation selectivity of color-responsive neurons in macaque V1. *J. Neurosci.* 28, 8096–8106.
- Jones, H.E., Grieve, K.L., Wang, W., and Sillito, A.M. (2001). Surround suppression in primate V1. *J. Neurophysiol.* 86, 2011–2028.
- Kiper, D.C., Fenstemaker, S.B., and Gegenfurtner, K.R. (1997). Chromatic properties of neurons in macaque area V2. *Vis. Neurosci.* 14, 1061–1072.

- Komatsu, H., Ideura, Y., Kaji, S., and Yamane, S. (1992). Color selectivity of neurons in the inferior temporal cortex of the awake macaque monkey. *J. Neurosci.* 12, 408–424.
- Lafer-Sousa, R., and Conway, B.R. (2013). Parallel, multi-stage processing of colors, faces and shapes in macaque inferior temporal cortex. *Nat. Neurosci.* 16, 1870–1878.
- Landisman, C.E., and Ts'o, D.Y. (2002a). Color processing in macaque striate cortex: electrophysiological properties. *J. Neurophysiol.* 87, 3138–3151.
- Landisman, C.E., and Ts'o, D.Y. (2002b). Color processing in macaque striate cortex: relationships to ocular dominance, cytochrome oxidase, and orientation. *J. Neurophysiol.* 87, 3126–3137.
- Lennie, P., Krauskopf, J., and Sclar, G. (1990). Chromatic mechanisms in striate cortex of macaque. *J. Neurosci.* 10, 649–669.
- Li, M., Liu, F., Juusola, M., and Tang, S. (2014). Perceptual color map in macaque visual area V4. *J. Neurosci.* 34, 202–217.
- Li, M., Liu, F., Jiang, H., Lee, T.S., and Tang, S. (2017). Long-Term Two-Photon Imaging in Awake Macaque Monkey. *Neuron* 93, 1049–1057.
- Lim, H., Wang, Y., Xiao, Y., Hu, M., and Felleman, D.J. (2009). Organization of hue selectivity in macaque V2 thin stripes. *J. Neurophysiol.* 102, 2603–2615.
- Livingstone, M.S., and Hubel, D.H. (1984). Anatomy and physiology of a color system in the primate visual cortex. *J. Neurosci.* 4, 309–356.
- Lu, H.D., and Roe, A.W. (2008). Functional organization of color domains in V1 and V2 of macaque monkey revealed by optical imaging. *Cereb. Cortex* 18, 516–533.
- Lu, Y., Yin, J., Chen, Z., Gong, H., Liu, Y., Qian, L., Li, X., Liu, R., Andolina, I.M., and Wang, W. (2018). Revealing detail along the visual hierarchy: neural clustering preserves acuity from V1 to V4. *Neuron* 98, 417–428.
- Martin, P.R., White, A.J., Goodchild, A.K., Wilder, H.D., and Sefton, A.E. (1997). Evidence that blue-on cells are part of the third geniculocortical pathway in primates. *Eur. J. Neurosci.* 9, 1536–1541.
- Mazer, J.A., Vinje, W.E., McDermott, J., Schiller, P.H., and Gallant, J.L. (2002). Spatial frequency and orientation tuning dynamics in area V1. *Proc. Natl. Acad. Sci. USA* 99, 1645–1650.
- Mehrani, P., Mouraviev, A., and Tsotsos, J.K. (2020). Multiplicative modulations enhance diversity of hue-selective cells. *Sci. Rep.* 10, 8491.
- Mollon, J.D. (2003). The origins of modern color science. In *The Science of Color*, S. Shevell, ed. (Elsevier), pp. 1–39.
- Mollon, J.D. (2009). A neural basis for unique hues? *Curr. Biol.* 19, R441–R442, author reply R442–R443.
- Namima, T., Yasuda, M., Banno, T., Okazawa, G., and Komatsu, H. (2014). Effects of luminance contrast on the color selectivity of neurons in the macaque area v4 and inferior temporal cortex. *J. Neurosci.* 34, 14934–14947.
- Nandy, A.S., Nassi, J.J., and Reynolds, J.H. (2017). Laminar Organization of Attentional Modulation in Macaque Visual Area V4. *Neuron* 93, 235–246.
- Nasr, S., and Tootell, R.B.H. (2018). Columnar organization of mid-spectral and end-spectral hue preferences in human visual cortex. *Neuroimage* 181, 748–759.
- Nauhaus, I., Nielsen, K.J., Disney, A.A., and Callaway, E.M. (2012). Orthogonal micro-organization of orientation and spatial frequency in primate primary visual cortex. *Nat. Neurosci.* 15, 1683–1690.
- Oostenveld, R., Fries, P., Maris, E., and Schoffelen, J.M. (2011). FieldTrip: Open source software for advanced analysis of MEG, EEG, and invasive electrophysiological data. *Comput. Intell. Neurosci.* 2011, 156869.
- Pan, Y., Chen, M., Yin, J., An, X., Zhang, X., Lu, Y., Gong, H., Li, W., and Wang, W. (2012). Equivalent representation of real and illusory contours in macaque V4. *J. Neurosci.* 32, 6760–6770.
- Rosenthal, I., Ratnasingam, S., Haile, T., Eastman, S., Fuller-Deets, J., and Conway, B.R. (2018). Color statistics of objects, and color tuning of object cortex in macaque monkey. *J. Vis.* 18, 1.
- Roy, S., Jayakumar, J., Martin, P.R., Dreher, B., Saalmann, Y.B., Hu, D., and Vidyasagar, T.R. (2009). Segregation of short-wavelength-sensitive (S) cone signals in the macaque dorsal lateral geniculate nucleus. *Eur. J. Neurosci.* 30, 1517–1526.
- Sanada, T.M., Namima, T., and Komatsu, H. (2016). Comparison of the color selectivity of macaque V4 neurons in different color spaces. *J. Neurophysiol.* 116, 2163–2172.
- Sani, I., Santandrea, E., Golzar, A., Morrone, M.C., and Chelazzi, L. (2013). Selective tuning for contrast in macaque area V4. *J. Neurosci.* 33, 18583–18596.
- Schroeder, C.E., Mehta, A.D., and Give, S.J. (1998). A spatiotemporal profile of visual system activation revealed by current source density analysis in the awake macaque. *Cereb. Cortex* 8, 575–592.
- Sincich, L.C., and Horton, J.C. (2005a). The circuitry of V1 and V2: integration of color, form, and motion. *Annu. Rev. Neurosci.* 28, 303–326.
- Sincich, L.C., and Horton, J.C. (2005b). Input to V2 thin stripes arises from V1 cytochrome oxidase patches. *J. Neurosci.* 25, 10087–10093.
- Smith, V.C., and Pokorny, J. (1975). Spectral sensitivity of the foveal cone photopigments between 400 and 500 nm. *Vision Res.* 15, 161–171.
- Solomon, S.G. (2002). Striate cortex in dichromatic and trichromatic marmosets: neurochemical compartmentalization and geniculate input. *J. Comp. Neurol.* 450, 366–381.
- Solomon, S.G., and Lennie, P. (2005). Chromatic gain controls in visual cortical neurons. *J. Neurosci.* 25, 4779–4792.
- Tanigawa, H., Lu, H.D., and Roe, A.W. (2010). Functional organization for color and orientation in macaque V4. *Nat. Neurosci.* 13, 1542–1548.
- Tootell, R.B.H., Silverman, M.S., Hamilton, S.L., De Valois, R.L., and Switkes, E. (1988). Functional anatomy of macaque striate cortex. III. Color. *J. Neurosci.* 8, 1569–1593.
- Ts'o, D.Y., and Gilbert, C.D. (1988). The organization of chromatic and spatial interactions in the primate striate cortex. *J. Neurosci.* 8, 1712–1727.
- Valverde Salzmann, M.F., Bartels, A., Logothetis, N.K., and Schüz, A. (2012). Color blobs in cortical areas V1 and V2 of the new world monkey *Callithrix jacchus*, revealed by non-differential optical imaging. *J. Neurosci.* 32, 7881–7894.
- Wade, A., Augath, M., Logothetis, N., and Wandell, B. (2008). fMRI measurements of color in macaque and human. *J. Vis.* 8, 6.1–619.
- Xiao, Y., Zych, A., and Felleman, D.J. (1999). Segregation and convergence of functionally defined V2 thin stripe and interstripe compartment projections to area V4 of macaques. *Cereb. Cortex* 9, 792–804.
- Xiao, Y., Wang, Y., and Felleman, D.J. (2003). A spatially organized representation of colour in macaque cortical area V2. *Nature* 421, 535–539.
- Xiao, Y., Casti, A., Xiao, J., and Kaplan, E. (2007). Hue maps in primate striate cortex. *Neuroimage* 35, 771–786.
- Xiao, Y., Kavanau, C., Bertin, L., and Kaplan, E. (2011). The biological basis of a universal constraint on color naming: cone contrasts and the two-way categorization of colors. *PLoS ONE* 6, e24994.
- Yoshioka, T., and Dow, B.M. (1996). Color, orientation and cytochrome oxidase reactivity in areas V1, V2 and V4 of macaque monkey visual cortex. *Behav. Brain Res.* 76, 71–88.
- Zweig, S., Zurawel, G., Shapley, R., and Slovin, H. (2015). Representation of Color Surfaces in V1: Edge Enhancement and Unfilled Holes. *J. Neurosci.* 35, 12103–12115.

STAR★METHODS

KEY RESOURCES TABLE

REAGENT or RESOURCE	SOURCE	IDENTIFIER
Experimental Models: Organisms/Strains		
Rhesus macaque (<i>Macaca mulatta</i>)	Beijing Institute of Xieerxin Biology Resource	http://www.xexbio.com/
Rhesus macaque (<i>Macaca mulatta</i>)	Beijing Prima Biotech	http://www.primasbio.com/cn/Default
Recombinant DNA		
AAV1.hSynap.GCaMP5g.WPRE.SV40	Penn Vector Core	V6270S
pAAV.Syn.GCaMP6s.WPRE.SV40	Chen et al., 2013	RRID:Addgene_100843
Software and Algorithms		
MATLAB	Mathworks	RRID:SCR_001622
Psychophysics Toolbox	http://psychtoolbox.org/	RRID:SCR_002881
Offline Sorter Spike Sortng Software	Plexon	RRID:SCR_000012
Fieldtrip Toolbox	http://www.fieldtriptoolbox.org	RRID:SCR_004849
Other		
Omniplex Recording System	Plexon	RRID:SCR_014803

RESOURCE AVAILABILITY

Lead Contact

Further information and requests for resources and reagents should be directed to and will be fulfilled by the Lead Contact, Wei Wang (w.wang@ion.ac.cn).

Materials Availability

This study did not generate new unique reagents.

Data and Code Availability

The complete dataset and MATLAB analysis code are freely available from the corresponding author upon request.

EXPERIMENTAL MODEL AND SUBJECT DETAILS

Fifteen adult rhesus macaques (*Macaca mulatta*, eleven males and four females, 3~7 years old, weighing 4.0–10.9 kg) were used in this study. All experimental procedures were approved by both Animal Committee of the Institute of Neuroscience, Chinese Academy of Sciences and Peking University Animal Care and Use Committee. All experimental procedures were also in accordance with the National Institutes of Health Guide for the Care and Use of Laboratory Animals.

METHOD DETAILS

Optical Imaging of Intrinsic-signal

All experimental procedures for primate research were approved by the Animal Care and Use Committee of the Institute of Neuroscience and by the local ethical review committee of the Shanghai Institutes for Biological Sciences. Eleven adult rhesus macaques (*Macaca mulatta*, seven males and four females, 4~7 years old, weighing 4.0~9.4 kg) were prepared and maintained for simultaneous optical imaging of intrinsic-signal (OIS) in V1, V2, and V4 as previously described (An et al., 2012; Pan et al., 2012). The optical recording chamber was centered over the lunate sulcus (LS), allowing for concurrent recording of optical signals from a field of view encompassing opercular V1, the full width of V2 that is exposed between V1 and the LS, and a hemicircular field of V4 extending across the prelunate gyrus (Pan et al., 2012; Tanigawa et al., 2010).

A gamma-corrected monitor (Sony G520, 1280x960 pixels, 100 Hz, luminance range from 0.1 to 80 cd/m²) was placed 57 cm from the eyes to subtend 40° × 30°. The monitor was calibrated by SpectroCAL MKII Spectroradiometer (Cambridge Research Systems). The fovea and other retinal landmarks for all subjects were back projected to the screen center using a reversing ophthalmoscope (Jones et al., 2001). Full-screen visual stimuli were generated with PSYCHTOOLBOX-3 running in MATLAB. For mapping the

orientation response domains, sinusoidal luminance gratings with orientation 0°, 45°, 90°, or 135° were presented at varied spatial frequency (0.125~6.0 cycles/degree, c/d) and temporal frequency (2~5 cycles/second, c/s). For the ocular dominance test identifying the V1/V2 border we presented the same gratings monocularly, to each eye in turn (An et al., 2012; Lu et al., 2018). In conformity with the stimulus protocols of previous studies (Landisman and Ts'o, 2002b; Li et al., 2014; Lu and Roe, 2008; Tanigawa et al., 2010; Xiao et al., 2007) we used dual color red/green and blue/yellow square-wave gratings to map the gross extent of chromatic response domains, each chromatic grating being contrasted with an achromatic grating of the same spatial frequency (SF) at 0.25 or 0.5 c/d (Figure 1C). To map the intrinsic hue-topography of chromatic response domains (“hue maps”), we contrasted seven single-color square-wave gratings with a similarly configured achromatic (gray/black) grating of matching luminance contrast and spatial frequency. The seven test colors and the gray phase of the achromatic grating were isoluminant ($\sim 11.20 \text{ cd/m}^2$) (Figure 1D). The seven hues comprising the test-set were red, orange, yellow, green, cyan, blue and purple, respectively (Figure 1A). These are the hues respectively specified by the angles 0°, 30°, 60°, 120°, 180°, 240°, and 300° in the chromatic plane common to the Hue-Saturation-Lightness (HSL) and Hue-Saturation-Value (HSV) perceptual color spaces. To generate isoluminant hue stimuli and take the monitor gamut into consideration, we used a spectroradiometer to ensure all the colors were isoluminant with proper RGB ratio (Evans et al., 1954). We further converted these colors into CIE 1931 color space for comparison with other studies (see details in Table S1); the cone excitations (in the MacLeod-Boynton chromaticity diagram) and cone contrasts of each all tested hue are calculated using 2-deg Smith & Pokorny cone fundamentals (Smith and Pokorny, 1975), and presented in Figure 1A and Table S1. The colors shown in the article figures are adjusted using pseudo-colors for better visualization.

Electrophysiological Recordings and Analysis

We trained two rhesus macaques (Macaca mulatta, two males, 6~7 years old, 6.9 and 10.9 kg) to do passive fixation tasks for the awake electrophysiology. The electrophysiological recording procedure using 16-channel multisite linear electrodes (U-probes with intercontact spacing of 150 μm) and Omniplex Recording System (Plexon) was described in our previous study (Lu et al., 2018). Stimuli were generated with PSYCHTOOLBOX-3 running in MATLAB on a gamma-corrected CRT monitor (Vision Master Pro-514, Iiyama; 1600 \times 1200 pixels at 100 Hz) placed 114 cm from eyes. An infra-red eye tracking system (Eyelink 1000, SR Research) was used to track the eye position at 500 Hz while the animal maintained fixation within a 1° window. Animals had to fixate on an isoluminant blank screen for 800 ms to initiate a trial and keep fixation for 1000~1500 ms during stimulus presentation. After the stimulus was turned off, the animal had to maintain fixation for another 500 ms. The raw electrophysiological data were sampled at 40 kHz. The data were later filtered with a 300 Hz high-pass Bessel 4 pole filter and multi-unit spikes were detected at ± 3.6 standard deviations using Offline Sorter software (Plexon). The LFP was filtered between 1 and 300 Hz. The data was further analyzed by Fieldtrip Toolbox (Oostenveld et al., 2011). The visual stimuli used were achromatic drifting sinusoidal gratings, static color patches and drifting sinusoidal color gratings, all either full-screen or sized to match the response fields of the recording sites.

As the response fields of neurons within a cortical column are similar in position and size (Nandy et al., 2017), we only took the response field of the most responsive channel to represent each penetration. We used either hand-mapping or computer-automated mapping with a grating patch to depict the response field of the penetration (Chen et al., 2014; Gallant et al., 1996; Lu et al., 2018; Mazer et al., 2002).

U-probes were inserted perpendicular to the cortical surface in areas V1, V2 and V4, in search of color domains where neural responses demonstrated predominant tuning to color stimuli. A neuron was deemed to be color selective if it had a differential response to the 7 hues tested ($p < 0.05$, ANOVA). We calculated the laminar current source density (CSD) with the second spatial derivative of the LFP response across layers in response to a flash stimulus (100 ms of the test hue, or white, followed by 900 ms black in each trial) (Hansen et al., 2011; Lu et al., 2018; Schroeder et al., 1998). We then full-wave rectified the CSD signals to color stimuli in the supragranular layers to obtain the rectified current (Chen et al., 2007; Schroeder et al., 1998). Due to the variance in the magnitude of currents in different cortical depths and penetration sites, we normalized the CSD amplitudes (in the period of 0~150ms after stimulus onset) within each recording channel to eliminate the variation among recording channels. The z-score normalized current amplitude were then compared among different color stimulation conditions. The orientation selectivity index (OSI) of the recording cell is defined as $\text{OSI} = (R_{\text{preferred}} - R_{\text{orthogonal}})/R_{\text{preferred}}$, where R is the cell's response (firing rate) to the preferred orientation or the orthogonal orientation. The color preference index (CPI) is defined as $(R_{\text{color}} - R_{\text{achromatic}})/(R_{\text{color}} + R_{\text{achromatic}})$, where R is the cell's response to the preferred color stimulus or preferred achromatic orientation.

Histological Cytochrome-Oxidase Staining

Three animals were perfused for conventional histological processing upon termination of optical-imaging. Tangentially oriented sections were cut through regions of the brain underlying the optical recording chamber. These were stained for cytochrome-oxidase (CO) to reveal blob and stripe compartments in areas V1 and V2, respectively, as performed in previous studies (An et al., 2012; Sincich and Horton, 2005b). The histological sections were co-registered with the optical images using as landmarks both the marked boundary of the cortical surface underlying the recording chamber and the location of the LS (An et al., 2012).

Two-photon Imaging and Analysis

Two adult (3~5 years old, 4~9kg) rhesus macaques were used in the 2-photon imaging experiment. These experimental protocols were approved by the Peking University Animal Care and Use Committee. Detailed procedures of surgery were described in previous

article (Li et al., 2017). Briefly, the animals were anesthetized and craniotomy was performed in the target brain area. The dura was opened, and an AAV vector (AAV1.hSynap.GCaMP5g.WPRE.SV40, Penn Vector Core or pAAV.Syn.GCaMP6s.WPRE.SV40, Addgene) (Chen et al., 2013) was injected at multiple cortical sites. The dura was then sutured, bone replaced and nailed, and skin sutured. About 1~2 months later, the cranial window was reopened and the dura was removed. The edge of a glass window was sealed beneath the dura, the bones and edge of the glass window being covered by dental cement. Finally, 3 head posts were mounted on the head (two in front and one in back), and a T-shape brace was connected to the 3 head posts to ensure structural integrity.

After a recovery period of 10 days from the second surgery, the animals were trained to maintain eye-fixation. 2-photon imaging was performed using a Prairie Ultima IV (*In Vivo*) 2-photon microscope (Bruker Nano, FMBU, formerly Prairie Technologies) with a Ti:Sapphire laser (Mai Tai eHP, Spectra Physics). The wavelength of the laser was set at 1000 nm. With a 16 × objective (0.8-N.A., Nikon), an area of 850 μm × 850 μm was imaged. The fast-resonant scan (up to 32 frames per second) was used to obtain images of neuron activity (8 fps by averaging each 4 raw frames).

During the task, the animal was seated in a primate chair with head restraint. The animal had to fix its eyes on a small white spot (0.1°) within a window of 1° for a minimum of 2 s to obtain a juice reward. Eye positions were monitored with an infrared eye-tracking system (ISCAN) at 120 Hz. Visual stimuli were generated by ViSaGe system (Cambridge Research Systems, UK) and a 21" CRT monitor (Sony G520, 80Hz refresh rate, maximum luminance, 105 cd/m²). The CRT was positioned 51cm from the eyes. We estimated the RF sizes and positions of the imaged neurons with small gratings and bars presented at different locations. We used two types of visual stimulus: a static closed circle (0.8° in diameter for V1, and V2) of a specific hue for testing hue preference, or an achromatic grating (size: 0.8° in diameter, spatial frequency: 2.5 c/d, temporal frequency: 2.2 c/s) for testing the cell 0.8° for V1 of varied orientation (0°, 30°, 60°, 90°, 120°, and 150°) for testing orientation preference. The visual stimulus was presented in the receptive field for 1 s after 1 s blank within the 2 s fixation period. For the regions of interests, we first search for visual responsive domains under low magnification lens (4 × objective) in response to our test stimuli. After we found the region with strong responses, we switched into high magnification lens (16 × objective) for detailed recording and mapping.

All data analyses were performed using customized MATLAB software (The MathWorks, Natick, MA). The images from each session were first realigned to a template image (the average image of 1000 frames in the middle of an imaging session) using a normalized cross-correlation-based translation algorithm, to correct the X-Y offset of images caused by the motion between the objective and the cortex. The 8 (125 msec) frames preceding stimulus onset, and 8 subsequent frames were separately averaged to form the respective OFF and ON frames of a stimulus. All ON and OFF frames of a stimulus were filtered by a small Gaussian filter ($\delta = 2 \mu\text{m}$) to remove very high frequency noise. All subsequent processing was based on these ON and OFF frames. Cells were extracted from an (ON-OFF)/OFF image of each stimulus condition by difference of Gaussian (DOG) filters, and all isolated pixels of a cell were averaged to calculate that cell's response. Each cell if significantly tuned (one-way ANOVA, $p < 0.05$) to one or more color in the testing seven hues was assigned as a hue selective cell. A cell if significantly tuned (one-way ANOVA, $p < 0.05$) to one or more orientation in the testing six orientations was assigned as an orientation selective cell. The preferred (maximum response) color (or orientation) is displayed on the cell distribution map. To generate density map of cells preferring each hue across the 850 μm square recording window, the locations of cells were first denoted by white dots (value = 1) against a black background (value = 0), then this map was submitted to an 2D averaging filter with square window of 0.125 × 0.125 mm² (step size: 1 pixel, 1.5625 μm). For each hue the cell number within the sliding window when centered on each pixel, divided by the area of the sliding window, represents the hue-specific cell density at that pixel.

We then used the hue-specific cell density maps to generate chromotopic hue maps from the 2-photon data comparable to those obtained from the intrinsic-signal data. First we removed cell noise: for each hue, we found the average cell density of all pixels with non-zero density, and discarded all pixels below a threshold set at 25% of the average density. Hue response loci were then delimited by contours of 75% peak cell density around each peak. Following this procedure, individual hues could return multiple loci; the final hue map comprised loci with the highest hue-specific peak cell density.

To test the spatial scale of cell-clustering according to feature preference in 2-photon imaging data, we computed the cluster index (Nauhaus et al., 2012) for orientation cells in V1 and color cells in V1 and V2. The cluster index is defined as:

$$\text{Cluster index } (d) = \frac{E(1 - r_{\text{resampled}})}{E(1 - r_{\text{actual}}|d)},$$

where d denotes the cortical distance between a pair of cells, r is the correlation coefficient between the tuning properties (either orientation or color feature) of a cell pair and E is the expected value. The cell resampling was performed 1000 times. Values of the cluster index above 1 or below 1 suggest, respectively, that the feature preferences of cell pairs at the prescribed distance are more similar or dissimilar than those of randomly paired neurons in the imaging window. The OSI and CPI are in the same definition as that in the electrophysiology, but cell's response is measured as the change in fluorescence (Garg et al., 2019).

Analysis of Intrinsic Signals

To generate a response map of intrinsic signal, single-condition maps were generated first. We averaged, across trials, a response frame due to the visual stimulation (R_1 , a period of 2~6 s from stimulus onset), and a blank frame (R_0 , the interval from 1.0 to 0.5 s before stimulus onset) to generate a single-condition map of reflectance change $\Delta R/R$ as $(R_1-R_0)/R_0$. A differential map was then generated by pixelwise subtraction of a contrasting pair of single-condition maps, such as orthogonal orientations (e.g., 0°-90°) or

chromatic versus achromatic gratings (e.g., red/green – black/white) (Bonhoeffer and Grinvald, 1996). Polar orientation preference maps were constructed using a vector summation algorithm. For visualization, the images were high-pass filtered (1~1.1 mm in diameter) and smoothed (170 μm in diameter) by circular averaging filters to suppress low- and high-frequency noise while avoiding signal distortion (An et al., 2012; Pan et al., 2012). A variability map was obtained to find pixels with large cross-trial variability (e.g., blood vessels and other noisy regions) and a mask was generated, based on an objectively chosen threshold (An et al., 2012; Lu et al., 2018; Pan et al., 2012).

For quantitative measurement of size, the perimeter of a response domain (as visualized in the differential map) was set at a criterion of 3 standard deviations above baseline. Baseline activity refers to the “response” in the second half of the blank frame, after equivalent processing through single condition and differential maps, its sampling distribution being determined across pixels in the differential map subsequent to spatial filtering and masking. The local cortical territory responsive to chromatic/achromatic contrast – that we term a “color-response blob” – was defined as the sum (or envelope) of the response domains pertaining to each of our seven single-hue stimuli under the criterion of mean+3SD.

The size measurement of CO blobs in V1 was based on a previously reported method (Sincich and Horton, 2005b) with two modifications. First, to minimize artifacts, we identified pixels with density level darker than darkest blob (stray lymphocytes) or brighter than brightest interblobs (blood vessels) in the CO stained image, and replaced these pixels with their average surrounding density. Second, we used a triangular filter (65 μm width at half-height) instead of Gaussian filter in the original method - to smooth the blobs, that we found better maintains blob shape. Finally, blob territory was designated as the darkest 33% of the region under examination. The measured blob sizes were multiplied by an areal correction index of 1.23 to compensate for tissue shrinkage during histology (Solomon, 2002). The diameters of CO blobs are also measured for comparison although the shape of blobs in V1 are not in perfect circles, we computed the diameter of a CO blob by averaging the length major and minor axes of the blob.

To quantify the accuracy of co-registration between images of CO staining and intrinsic optical imaging, we aimed to measure the average distortion distance of corresponding blobs in CO staining and optical imaging (Valverde Salzmann et al., 2012). In detail, we measured the position of peak density for each CO blob, and generated the position coordinates of response blobs by averaging the peak response positions across all the hue stimuli we tested. Due to tissue shrinkage during stepwise histological processing, it is not applicable to directly compare the blob positions in CO staining with those obtained by intrinsic optical imaging. Thus, we calibrated the CO position matrix by linear fitting to the position matrix from intrinsic optical imaging so as to quantify the differences between these two matrices. We discarded blobs along blood vessels due to the serious distortion of their positions and generated a final averaged distortion distance between corresponding blobs in CO staining and intrinsic imaging.

To assess the relative level of response to each hue we defined a quantity termed hue “response power” as the product of the response strength and size for each single-hue response domain (or “hue-spot”). As before, the size of the hue-spot was determined by the number of pixels above the mean+3SD threshold, and strength is the mean response strength of those pixels. The “power ratio” of a particular hue within a given color-response blob was defined as that hue’s response power divided by the sum of all hue response powers within the blob. This ratio is frequently zero, for hues that fail to register a super-threshold response in a particular blob; all such null instances were included in calculating the global, mean power ratios that we report for each area. We tested the uniformity of response power distribution in each area, and compared the uniformity between areas by a bootstrap method, as follows. For testing the uniformity of hue response distribution in an individual cortical area: (i) we randomized the response powers for each blob, i.e., reassigning hue labels by randomly rotating through 1-7 positions, to preserve the circularity of color space; (ii) we averaged across blobs and found the variance of the averaged, randomized response powers within an area; (iii) we did this 10^6 times in order to rank the actual empirical variance for that area within the randomized outcomes, and hence calculate P. If hue bias within an individual blob were due to random noise, we would expect it to cancel out in the average across all blobs within an area. For testing differences in the uniformity of response power distribution between two areas: we followed steps (i) and (ii) as above for each area separately, yielding a difference in variance between areas for each iteration. Multiple iterations (10^6) gave a population of variance differences, within which we ranked the actual difference between areas obtained with the empirical data.

To examine hue topography, we systematically measured the proportional overlap between all possible pairings of our seven single-color test-hues. Again, counting only super-threshold pixels (mean+3SD), we calculated the overlap ratio as the proportion of pixels dually responsive to specific hue pairs within a single hue-spot: i.e., the territory of each hue-spot was assigned to a fraction uniquely activated by that hue, and upto six other partially overlapping fractions jointly active with another hue. To better visualize the difference of overlap ratios between a pair of areas, we directly subtracted the overlap ratios of corresponding hue pairs and applied a color scale to the outcome. For graphical presentation of hue topography we drew contours around “peak response zones,” namely pixels thresholded at 0.75 times the maximum strength of each particular hue response within the host color blob, and also above the criterion of mean+3SD (Li et al., 2014; Xiao et al., 2003, 2007).

For a quantitative assessment of hue topography (i.e., the spatial parameters of chromotopic organization, Figure S5B), we used regression analysis of cortical distance against hue distance. Cortical distance was measured between all pairings of the peak points activated by each hue within a given color-response blob (affording regression of 21 data points for a complete map of 7 hues). Regression of each cortical hue map was measured in respect to three color metrics: (1) a linear hue metric, with hue angles 30°-330°, formed by a linearized hue circle (Figure S5C, upper). The function relating peak-to-peak cortical distance (y) to hue angle (x) is $y = a + b \cdot x$. Regression analysis was performed for all possible positions of the discontinuity within the hue circle; the position generating the maximal coefficient of determination (R^2) was selected, and the corresponding P value was adjusted by Bonferroni

correction for multiple comparisons (depending on the empirical number of hues in the hue map under examination). (2) a circular hue metric, with hue-angles 30°–180° ([Figure S5C](#), lower). This metric assessed correspondence to geometric length between loci on the hue circle (a sinusoidal function of hue angle) and the function relating peak-to-peak cortical distance to hue angle is $y = a+b\sin(x/2)$. (3) a metric derived from CIELab color space, specifically planar hue distances as specified by the DE76 metric ([Hunt and Pointer, 2011](#)) ; the function relating peak-to-peak cortical distance to hue distance is $y = a+b\cdot x$. The regression coefficient, and slope provided indices of chromotopic precision, and scale, respectively. Note that hue maps with less than four different hue-spots were excluded from analysis due to inadequate sample size ([Li et al., 2014](#)).

For an overall measure of the significance of chromotopic organization instanced in each hue map, we combined the p value obtained from regression with further bootstrap statistics, termed a randomization test and a permutation test, as described in a previous study ([Li et al., 2014](#)). For the randomization test, we resampled the cortical position of each hue response within a 1000×1000 matrix, and performed linear regression analysis for the distances of resampled positions (x) against the empirical hue distances (y). For the permutation test, the hue tags of peak points were randomly shuffled and the empirical cortical distances were regressed against the resampled hue distances. Each process repeated for 1000 times generating 1000 values of resampled coefficients of determination (R^2). The empirical R^2 was then ranked within each population of resampled R^2 values, to yield two additional p values. For the purpose of inter-area comparison, hue maps were accepted as displaying significant chromotopic organization if they attained a threshold level of significance across all three tests ($p < 0.05$ for regression, randomization test and permutation test). Finally, the proportions of significant chromotopic maps was compared among areas using a χ^2 test.

QUANTIFICATION AND STATISTICAL ANALYSIS

The n numbers are reported explicitly in the main text or figure legends. The statistical tests used were described in detail in the [Methods Details](#) subsection for each assay and in the relevant figure legends.